2016

Development of a Blast-Induced Damage Assessment Framework for Use in Threat Dependent Progressive Collapse Analyses

Matthew Jonathan Gombeda
Lehigh University

Development of a Blast-Induced Damage Assessment Framework for Use in Threat Dependent Progressive Collapse Analyses

by

Matthew Jonathan Gombeda

A Thesis

Presented to the Graduate and Research Committee

of Lehigh University

in Candidacy for the Degree of

Master of Science

in

Structural Engineering

Lehigh University

May 2016

This thesis is accepted and approved in partial fulfillment of the requirements for the Master of Science.

_____
Date

_____
Clay J. Naito
Thesis Co-Advisor

_____
Spencer E. Quiel
Thesis Co-Advisor

_____
Panayiotis Diplas
Chairperson of Department

ACKNOWLEDGEMENTS

The author would like to first thank his family, especially his parents Mark and Paula and sister Jenna, for all their encouragement throughout his studies. Without their constant love, prayers and support, this thesis would not have been possible. He would also like to extend much gratitude to all his friends and colleagues at ATLSS Engineering Center for their friendship and support; Corey Fallon, Christina Cercone, Omar Alawad, Alysson Mondoro, Matthew Horner, Frank Artmont, Aman Karamlou, Katelyn Kitner, Bhavana Valeti and so many others. He also would like to thank all of the faculty and staff in the Department of Civil and Environmental Engineering and at ATLSS for their support.

The author is greatly indebted to his advisors, Dr. Clay Naito and Dr. Spencer Quiel, for their continued guidance throughout his studies. Their constant reassurance and encouragement made the completion of this thesis much more enjoyable. The author feels so very privileged to have the opportunity to work with both of them.

Special thanks is also given to both the Precast/Prestressed Concrete Institute and the National Science Foundation for providing the funds necessary to finance the completion of this degree.

Since the completion of this thesis encompasses all knowledge and experience gained thus far in structural engineering, the author also wishes to thank all of his former educators, advisors, mentors and friends at Penn State University, most notably Dr. Jeffrey Laman, Mr. Thomas Skibinski, Dr. Daniel Linzell, Dr. Maria Lopez de Murphy, Dr. Farshad Rajabipour and Dr. Harry West. Their teaching at the undergraduate level provided the necessary foundation for the continuation of my studies in graduate school.

All praise, glory and honor to Jesus Christ the Lord.

TABLE OF CONTENTS

LIST OF TABLES

TABLE OF FIGURES

ABSTRACT

This paper proposes a methodology for mapping structural damage onto building frames due to exterior blast threats for use in a threat dependent progressive collapse assessment. The proposed approach contrasts with current practice, which typically relies on a threat-independent approach for progressive collapse analysis. Damage is mapped to the structure based on the calculated response of the discrete structural components (particularly the columns) to a blast-induced pressure time history. Contours of structural damage can then be mapped over the building face for discrete combinations of charges and standoffs. For a prototype reinforced concrete building frame, calculated distributions of damage for conventional explosive threats suggest that the current state of practice approach (in which damage is represented with a single column removal) may not constitute a generally conservative strategy for progress collapse resistant design. A set of uniform pushdown progressive collapse analyses was performed to assess the robustness of the prototype building frame when subjected to a spatial distribution of blast-induced damage relative to its intended design loads. The proposed framework can be used to determine standoff distances needed to reduce progressive multi-column failure scenarios in building frames for high-risk facilities and can be used as input for a progressive collapse assessment of these frames.

INTRODUCTION

In recent years, acts of domestic and international terrorism have resulted in the notable damage and/or collapse of several structures. Though relatively infrequent, blast or impact hazards due to terrorism can yield extensive amounts of property damage and, more importantly, loss of human life. Blast hazards are characterized by large local intensity, and the resulting damage has a high potential to cause a disproportionately large degree of structural collapse. Since the risk of terrorism is generally lower than that of natural disasters, buildings with higher damage consequences are the most appropriate candidates for the implementation of special mitigation strategies (Stewart 2008). Both the load and the resulting response due to intentional blast threats carry large degrees of uncertainty due to their extremely dynamic nature, the unpredictability of the location and magnitude, and the intelligent adaptability of the aggressors (Stewart et al. 2006).

Increased recognition of these levels of uncertainty within the construction industry has spurred the implementation of threat-independent approaches for mitigating progressive collapse due to local damage. Progressive collapse is defined as the "spread of an initial local failure from element to element, resulting eventually in the collapse of an entire structure or a disproportionately large part of it" (ASCE 2010). The current methodologies published by the US Government (GSA 2013; DoD 2013b) effectively decouple the direct effects of the loads which induce local damage from the performance of the locally damaged structure. The most common design approach used to mitigate the effects of progressive collapse is the alternate path method (APM), in which a structure is designed to bridge over its locally damaged portions. When using APM for building frames, the structure is subjected to the instantaneous removal of a single one-story column

at several critical locations; the system is then analyzed to determine if the remaining structure is able to "bridge" over the removed column and avoid collapse (see Figure 1). The column is notionally removed without any correlation to a potential hazard that caused its removal, and the remainder of the structure is considered to be undamaged. If the structure can redistribute its gravity loads in accordance with specified performance limits after the column removal, it is then considered to be resistant to progressive collapse. The use of APM to resist collapse due to simultaneous damage in multiple columns (unless they are in very close proximity) is not considered as a design objective in current guidelines (GSA 2013; DoD 2013b).

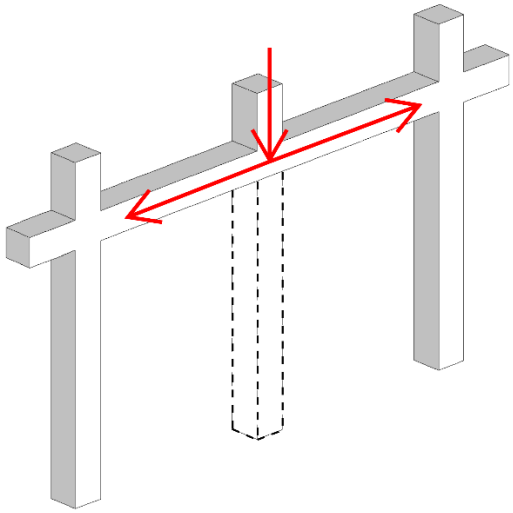

Figure 1 - Single column removal scenario for APM analysis

The question is often raised as to whether the single column removal with no damage to neighboring elements provides a realistic representation of structural damage due to a specified hazard. For the case of impact from a truck or small aircraft, the loss of a single column may be a reasonable representation. For the case of a blast load, however, damage could potentially result in critical or partial damage to two or more columns based on the size and location of an explosive threat. If such threats are considered credible design

scenarios for the building of interest, the extent of their blast effects may defeat the mitigation implemented via the APM, thus rendering the structure susceptible to progressive collapse. The potential for damage patterns that are not consistent with the single column removal has generated increased interest in the implementation of a *threat-dependent* progressive collapse analysis approach (Myers and Crawford 2014).

This paper examines the potentially unconservative nature of the single column removal for progressive collapse resistant design when considering the damage patterns created by blast loads. The proposed threat-dependent approach first generates contours of blast demands on the building envelope resulting from an explosive threat located at ground level outside the building. Columns are more susceptible than floor systems to exterior blast loads, and their blast-induced response (and potential resulting damage) is therefore the focus of this paper. The blast pressure time history experienced by each column is individually calculated based on its standoff and orientation to the specified explosive charge, which is represented in equivalent weight of TNT. Damage levels are calculated by comparing the reflected pressure (P_r) and impulse (I_r) at each column with its *P-I* resistance function, which is obtained using industry standard blast design tools (USACE 2008). When neighboring columns are examined together, the collective damage pattern enables an evaluation of the relevance of the single column removal scenario. This study uses a prototype building frame constructed of reinforced concrete but may be easily modified to accommodate other systems, including precast concrete and structural steel. The proposed framework can be used to determine appropriate standoff distances needed to prevent multi-column damage scenarios due to design basis blast threats.

BACKGROUND

Current US Government design guidelines for progressive collapse resistance (GSA 2013; DoD 2013b) have been developed in response to several recent events, in particular the 1995 bombing and collapse of the Murrah Federal Building in Oklahoma City, OK (Mlakar et al. 1998). The extent of blast-induced structural damage to the Murrah Building highlighted the need for redundancy and alternate load paths to resist progressive collapse (Byfield and Paramasivam 2012). Following their forensic investigation of the Murrah Building's collapse, Corley et al. (1998) noted that special moment frame or compartmentalized construction would have a greater ability to resist progressive collapse. Special moment frame detailing, in particular, was recommended as a method to mitigate both the damage due to the initial blast as well as the potential for subsequent collapse from blast-induced local damage (Corley et al. 1998).

In current practice, progressive collapse resistant design is typically performed via the APM direct design approach for several damage scenarios. To simulate each scenario, a column is removed one at a time in one-story lengths at several plan and elevation locations. When a column is removed, beam-to-beam continuity over that column is assumed to be preserved (see Figure 1), and no other damage is imparted to the structure. The structure is iteratively analyzed and strengthened for each removal scenario until the prescribed performance limits are met. The current threat-independent APM approach provides design professionals with a straightforward procedure in which the robustness of the structure is presumably increased. Nair (2006) explored a collection of recommendations from government standards and design guides for their significance on progressive collapse mitigation; all of the approaches included in that review did not

explicitly include the hazard which causes the initial damage. To implicitly consider the threat, the current criteria documents state that they are to be used in conjunction with the relevant blast-resistant design criteria that are associated with that agency and the building's level of design (GSA 2013; DoD 2013b).

Since the Murrah Building investigation, researchers have increasingly suggested that the single column removal scenario (with no other structural damage whatsoever) may not be representative of the damage pattern produced by a realistic blast threat. The results of the Murrah investigation (Mlakar et al. 1998) indicated that multiple columns failed due to the 1995 blast. However, the investigation suggested that the use of special moment frame detailing would have prevented all but one of the columns (G20) from failing suddenly due to the initial blast (Corley et al. 1998). Research by Bao and Li (2010), which examined the post-blast residual axial capacity of reinforced concrete columns, confirmed that the implementation of seismic detailing increased the column resistance to blast effects and, by extension, decreased the potential for progressive collapse.

The results of the Murrah Building investigation (Corley et al. 1998; Mlakar et al. 1998), however, did not consider whether the damaged columns which survived the blast would have been able to carry the redistributed loads from the failed column to resist progressive collapse. Kazemi-Moghaddam and Sasani (2015) recently revisited the event and performed an analytical study in which column G20 was removed suddenly but the remainder of the structure was undamaged. The results suggested that the structure would have resisted progressive collapse if only a single column had been removed due to the rapid dissipation of axial load in the column directly above the removal as well as load redistribution through Vierendeel action in the adjacent framing. This study indicated that

the initial blast-induced damage to the Murrah Building must have been more severe than a sudden removal of only a single column, thereby confirming the conclusions of the initial investigation (Corley et al 1998). Collectively, these studies suggest that a holistic evaluation of the progressive collapse potential of a building structure may not be possible without an evaluation of the extent of damage due to potential blast threats.

In the last decade, multiple research studies have expanded beyond the one column removal to consider the collapse consequences of a wider, more realistic extent of blast-induced damage. Studies by Sasani (2008) and Sasani et al. (2011) have examined the collapse resistance of building structures using damage scenarios with the removal of more than one column. These studies were performed under the assumption that a realistic blast threat may cause more extensive initial damage than considered by the current guidelines. However, the effects of the blast (particularly the damage caused to the neighboring elements) are not explicitly considered, similar to the aforementioned study by Kazemi-Moghaddam and Sasani (2015).

According to Starossek and Haberland (2010), the probability of the occurrence of progressive collapse is defined as a function of structural robustness, component vulnerability, and building exposure. Though convenient in its implementation, the current state of practice only addresses the influence of building robustness on the risk of collapse. To better address all three aspects of the collapse risk, several recent studies of progressive collapse resistance have explicitly incorporated the vulnerability and extent of damage for structures subjected to blast loading. McConnell and Brown (2011) performed an analytical study to monitor the response and progressive collapse vulnerability of steel columns subjected to the direct effects of blast loading for three failure criteria: stability, yielding,

and fracture. The results showed that the removal of only one column is highly non-conservative when designing for the possible effects of large charge sizes and that the alternative load path method for progressive collapse analysis is generally representative of relatively small charge sizes. Quiel et al. (2015) developed a correlation between the intensity of blast loading, the measure of collapse consequence to the building frame, and the extent of potential post-blast damage. The framework proposed in that study quantified the increasing extent of blast damage for a range of increasing charge sizes and/or decreasing standoffs, with the goal of identifying damage scenarios that extend beyond a single column removal. For a reinforced concrete frame, Shi et al. (2010) calculated the response of columns adjacent to those that were removed; by showing that their initial conditions were non-zero, the study demonstrated that removing a column is not a static case since some adjacent columns were not completely unaltered. Other studies such as Luccioni et al. (2004), Asprone et al. (2010), and Kelliher and Sutton-Swaby (2012) have also assessed the potential for structural collapse based on the extent and severity of damage produced by a range of blast threat locations and intensities.

PROPOSED FRAMEWORK

In order to assess the extent of blast-induced damage to a building frame as input for a progressive collapse analysis, a threat-dependent procedure has been developed by the authors. The flowchart shown in Figure 2 depicts the proposed five-step framework. The building frame is first designed in step 1 for conventional loads, followed by assessments of the structure's capacity to resist blast loads in step 2. The blast hazard is then assessed in step 3, and the corresponding blast-induced damage states are determined

in step 4. Steps 1-4 provide the initial conditions needed to conduct a progressive collapse analysis of the building in step 5.

The proposed framework ultimately determines the damage state at the end of the blast phase for each column on the building perimeter when exposed to a known explosive charge size at a given standoff distance. The damage states for all perimeter columns can be plotted as contours over the surface of a reinforced concrete building frame to visually represent the extent of damage and facilitate an assessment of the applicability and conservatism of the one column removal approach. A similar damage mapping technique was used by Netherton and Stewart (2009) to examine the extent of blast-induced damage and associated safety hazards for window glazing.

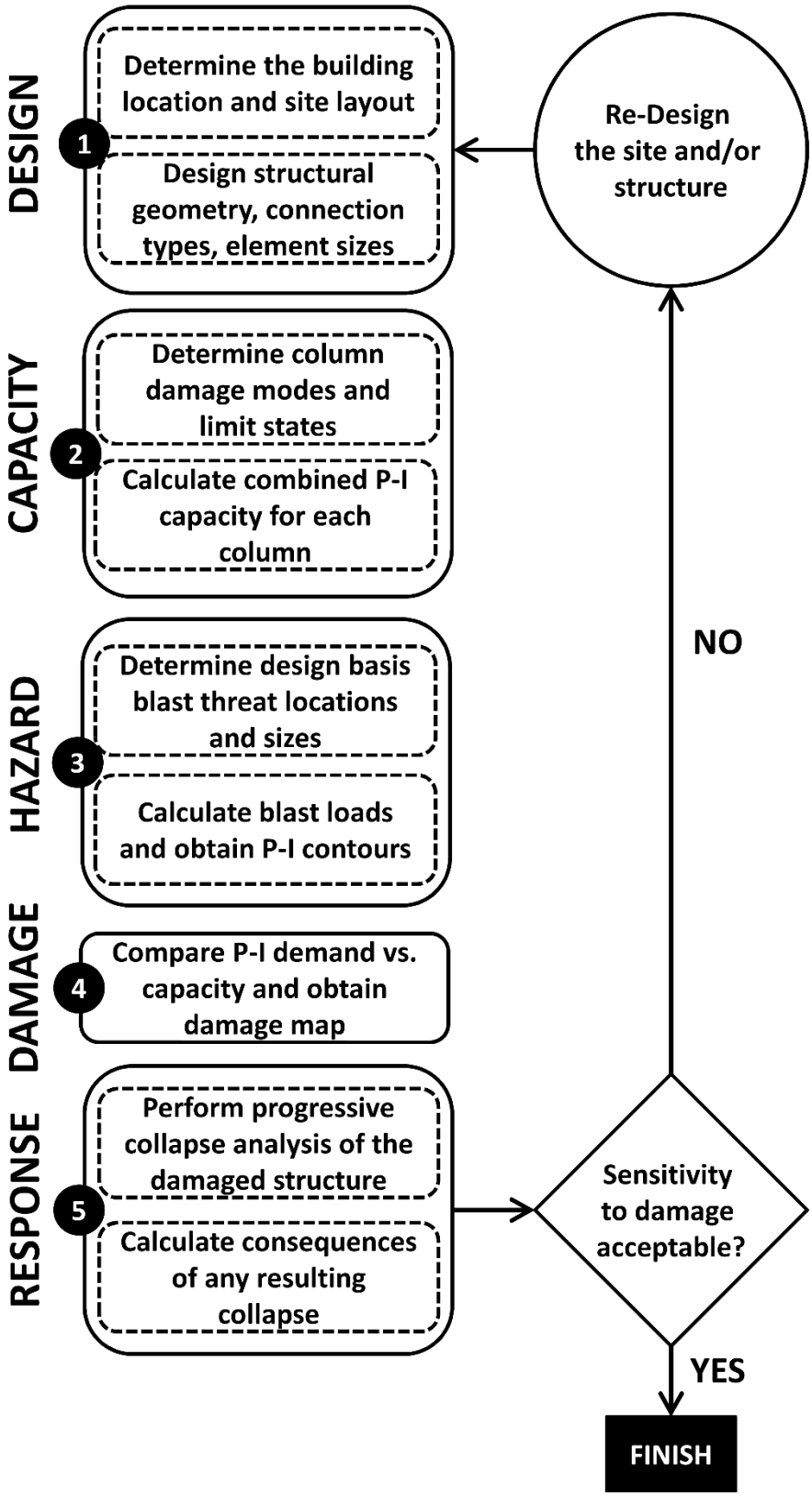

Figure 2 - Proposed threat-dependent framework for evaluating collapse resistance

Step 1: Design

For new construction, the proposed framework begins with the selection of the building's location and site layout as well as function and/or occupancy. Together, these characteristics establish the risk of having an intentional or accidental blast as well as the magnitude and proximity of a blast event. In this study, a generic site location and layout is chosen such that any magnitude or location of a blast threat is possible. The building is then designed for gravity loads as well as relevant loads resulting from natural hazards (e.g. earthquake, wind, flood, snow, etc.) in accordance with the International Building Code (ICC 2012) and ASCE 7-10 (ASCE 2010). When required, blast resistant design in accordance with government criteria (DoD 2013a) could also be performed during this step. For an existing building, this step would involve the acquisition of structural drawings and an evaluation of the as-built conditions needed for subsequent steps.

Step 2: Capacity Assessment

To determine a threat-dependent response of a reinforced concrete frame subjected to blast, the modes of damage must be defined. Assuming that the integrity of the beams is maintained by the adjacent floor diaphragms, the focus can be placed on the columns. Three potential modes are identified: breach, flexure, and direct shear.

Breach Resistance

Breach of a concrete column is defined as the complete loss of concrete through the depth of a cross-section (Williamson et al. 2010). Since this produces a through-thickness failure, breach is evaluated before the flexure and direct shear response criteria. Due to the large concentrated pressures required to breach a reinforced concrete member, this failure mode is commonly associated with close-in blast demands.

To quantify the breach potential of a reinforced concrete frame, the empirical breach threshold curve equations, shown as Equations (1), (2), and (3), were adopted from UFC 3-340-02 (DoD 2014).

$$\frac{h}{R} = \frac{1}{a + b\Psi + c\psi^2} \tag{1}$$

$$\psi = R^{0.926} f'c^{0.266} W_{adj}{}^{-0.353} \left(\frac{W_{adj}}{W_{adj} + W_c} \right)^{0.333} \tag{2}$$

$$W_{adj} = B_f C_f W \tag{3}$$

The equations use English units where *h* is the depth of the column in ft; *R* is the charge standoff distance in ft; *a*, *b*, and *c* are constants equal to 0.028205, 0.144308, and 0.049265, respectively; *f'c* is the compressive strength of concrete in psi; W_c is the explosive casing weight in *lb*, if applicable; B_f is equal to 1.0 for surface bursts; C_f is equal to 1.0 for spherical charges; and *W* is the equivalent TNT charge weight in *lb*. Given a column with known geometric and material properties, the greatest standoff distance at which breach can occur for a given quantity of TNT can be calculated. The corresponding scaled distance is used to determine the reflected pressure and impulse value at that point. Breach threshold curves can be developed for each column type as a function of TNT charge weight, pressure, and impulse, allowing for rapid assessment of performance. A specific example of this will be shown later in this paper.

Flexural Resistance

Flexural performance is assessed using standardized resistance functions (DoD 2014) and a generalized single degree of freedom (SDOF) analysis approach as discussed in Biggs (1964). Each column is equated to a mass-spring system and is allowed only one translational degree of freedom in the horizontal (parallel to the ground) direction as shown

in Figure 3a. Axial load is accounted for and is based on the location of the column within the structure. Applied axial load typically increases the moment capacity of the column because the applied compression stress offsets some of the tension in the reinforcing steel caused by flexure. The compression stress also helps to delay the onset of cracking. Conversely, the eccentricity of the applied axial load typically increases the applied moment. Also, the combined action of the axial load (P) and the lateral midspan deflection caused by flexure (Δ) causes an additional applied moment known as the "P-Δ" moment.

To consider a combination of axial load and dynamic inelastic lateral loading, an equivalent lateral load (ELL) approach is implemented. The approach consists of a time history analysis of the component that is subjected to blast loading. The axial load supplements the blast load with an ELL at each time step as shown in Figure 3b. This ELL represents an applied moment equal to the second-order moment from the "P-Δ" effect, where P is the total applied static and dynamic axial load at the time step and Δ is the maximum component deflection at the time step. The ELL is added to the blast load at the next time step. The ELL is calculated assuming the same load distribution as the input blast load (e.g. uniformly distributed pressure load) so that it can directly be added to the blast load. Figure 3c and 3d show the column modeled as an SDOF system with and without the inclusion of axial load effects, respectively. This approach allows for the inclusion of both static axial loads from gravity effects as well as the addition of dynamic axial demands, which are generated from the blast response of the roof component supported by the load-bearing component. The ELL method is accepted in classical theory

for analysis of load-bearing components with combined lateral load (Timoshenko and Gere 1961).

For continuous frames, the columns can be modeled with fixed-fixed, fixed-simple, or simple-simple boundary conditions. The choice of boundary condition is dependent on the detailing of the system and the goal of the analysis (i.e., estimation of peak reactions or deformations). The choice of boundary conditions determines the number of hinges formed during loading. As an example of the progression of failure, a fixed-simple condition would allow for the formation of two flexural plastic hinges. For a member with uniform reinforcement and cross-section, the first plastic hinge forms at the fixed support as the highest moment will develop at that location. After this hinge has formed, the beam will exhibit reduced stiffness and will behave as simply-supported until the moment at midspan exceeds the plastic moment capacity. Figure 3e shows the order of plastic hinge formation used in the model. In the figure, $R(x)$ is the resistance of the SDOF system as a function of displacement along the x-axis; M is the equivalent mass of the system; $P(t)$ is the laterally applied reflective pressure load as a function of time, t; γDL and γLL are the factored dead and live floor loads, respectively; $P2(t)$ represents any time dependent axial load; and e is the eccentricity of the applied floor load reaction on the column.

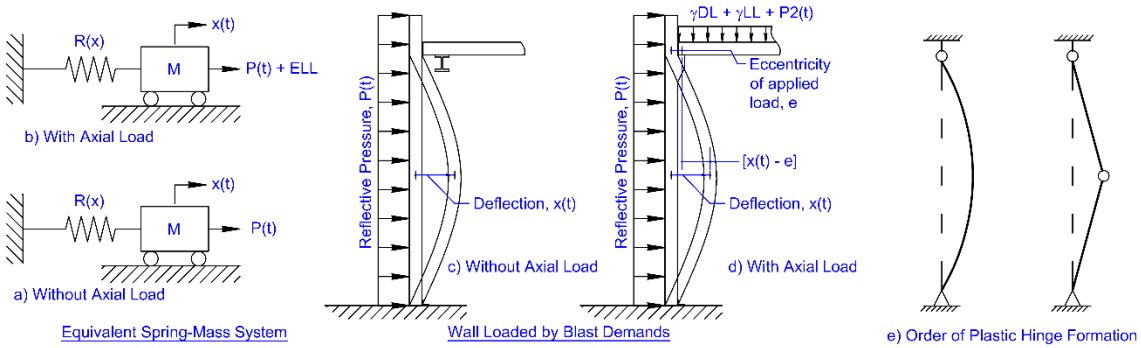

Figure 3 - Structural component and equivalent SDOF spring-mass system with plastic hinge formation order

To evaluate the flexural limit states of the columns, response criteria were adopted from references published by the US Army Corps of Engineers (USACE 2008b). These limits are given in terms of ductility and effective support rotation. Ductility, μ, is defined as the ratio of the blast induced deflection to the yield displacement at midspan. Midspan displacement can also be normalized with respect to length of the member, converting it into an effective support rotation, θ, which is approximated by Equation (4).

$$\theta = \tan^{-1}\frac{2\Delta}{L} \tag{4}$$

where Δ is the lateral deflection of the column at midspan, and L is the height of the column. Four response limits, B1 through B4, are summarized in Table 1. The physical interpretation of the damage levels bounded by these four response limits are defined in Table 2.

Table 1. Flexural response limits for reinforced concrete elements (USACE 2008b)

B1		**B2**		**B3**		**B4**	
μ	θ	μ	θ	μ	θ	μ	θ
1	N/A	N/A	4°	N/A	6°	N/A	10°

Table 2. Flexural damage level descriptions (USACE 2008b)

Component Damage Level	**Relationship to Response Limits**	**Description of Component Damage**
Blowout	Response greater than B4	Component is overwhelmed by the blast load causing debris with significant velocities
Hazardous	Response between B3 and B4	Component has failed, and debris velocities range from insignificant to very significant
Heavy	Response between B2 and B3	Component has not failed, but it has significant permanent deflections causing it to be unrepairable

Moderate	Response between B1 and B2	Component has some permanent deflection. It is generally repairable, if necessary, although replacement may be more economical and aesthetic
Superficial	Response is less than B1	Component has no visible permanent damage

Direct Shear Resistance

If a column does not initially breach, its direct shear resistance is determined by examining the column's dynamic rigid body motion which occurs prior to its flexural response. The rigid body motion behavior translates into a high concentration of shear stresses near the supports. To model the direct shear behavior of the columns, a resistance function relating shear stress to shear slip accounting for compression and rate effects was adopted from Krauthammer et al. (1986) and is shown in Figure 4. Using this model, the shear slip and resistance at each performance event is calculated and taken as a direct shear response limit for the column. As the column experiences greater shear slip the damage near the supports results in a reduction of stiffness. As the direct shear slip is currently uncoupled from the flexural behavior, the framework does not account for a reduction in flexural capacity caused by the slip induced weakening of the rigidity at the supports.

Alternate methods for shear assessment were found to be unconservative and are not used in this framework. This includes the UFC 3-340-02 (DoD 2014) approach which allows for direct shear to be considered as a result of flexural behavior. The UFC method does not account for the rigid body motion prior to the onset of bending. Dragos et al. (2014) showed that flexural bending occurs as shear slip is being developed. This results in higher resistance to shear failure modes. For simplicity, and to be conservative, the shear response is decoupled from the flexural response and the rigid body approach is

implemented. Future research will explore the interaction of shear slip with the ensuing flexural response.

The critical values of shear slip, i.e. the values of shear slip at which the resistance curve changes slope as seen in Figure 4, were used as the response limits for direct shear. The formulae used to calculate the shear slip and corresponding shear stress for each response level are shown in Equations (5) through (11). The values of slip at the first three response limits are previously defined by Krauthammer et al. (1986) and are given as 0.1 mm, 0.3 mm, and 0.6 mm for Δ_{DS1}, Δ_{DS2}, and Δ_{DS3} respectively. The other displacement limits are determined in accordance with Equations (9) and (11).

$$\tau_{DS1} = 231 + 0.220f'c \tag{5}$$

$$\tau_{DS2} = 11.2\sqrt{f'c} + 1.12\rho_{vt}f_y \leq 0.35\, f'c \tag{6}$$

$$\tau_{DS3} = \tau_{DS2} \tag{7}$$

$$\tau_{DS4} = \frac{1.19A_{sb}f_s'}{A_c}\text{s} \tag{8}$$

$$\Delta_{DS4} = \Delta_{DS3} + \frac{\tau_{DS3} - \tau_{DS4}}{2000 + 0.75f'c} \tag{9}$$

$$\tau_{DS5} = \tau_{DS4} \tag{10}$$

$$\Delta_{DS5} = 2\left(\frac{(e^x) - 1}{120}\right), where\ x = \frac{900}{2.86\sqrt{\frac{f_c'}{d_b}}} \tag{11}$$

ρ_{vt} is the longitudinal reinforcement ratio; $f'c$ is the concrete compressive strength in psi; f_y is the yield strength of rebar in psi; A_{sb} is the area of primary tension reinforcement in square inches; f_s' is the ultimate tensile strength of rebar in psi; A_c is the cross-sectional area of the column in square inches; and d_b is the rebar diameter in inches. The shear stress corresponding to each response level, i, is then multiplied by twice the cross sectional area (which accounts for both supports) of the member to obtain shear force, which is then divided by the tributary surface area of the member face to calculate the shear resistance,

R_{DSi}, as shown in Equation (12), where A_{trib} is calculated using either Equation (14) or (15). The influence of axial load is accounted for by increasing the direct shear resistance function values in accordance with ACI 318 (2011) for members under axial compression, as shown in Equation (13) and modeled after work done by Astarlioglu et al. (2013), where R'_{DSi} is the enhanced, axial load influenced direct shear resistance at response level, i; and P_u is the total factored column axial load. Since the total column axial load varies over the height of the building, a set of direct shear resistance values must be calculated for each building story. The resulting resistance function is then used as input for the dynamic analysis.

$$R_{DSi} = \frac{2\tau_{DSi}A_c}{A_{trib}} \tag{12}$$

$$R'_{DSi} = (1 + \frac{P_u}{2000A_c}) \times R_{DSi} \tag{13}$$

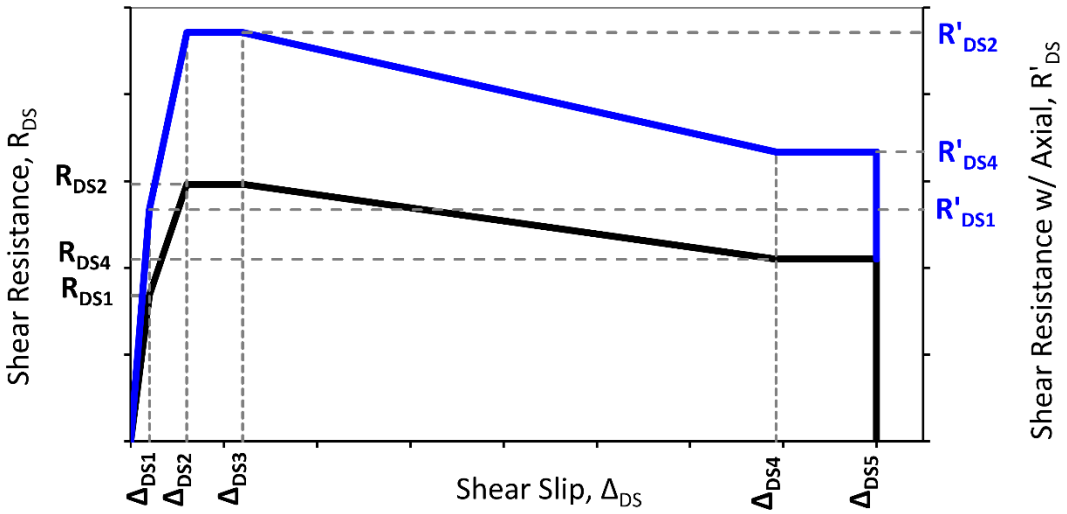

Figure 4 - Plot of direct shear slip resistance function showing the locations of response limits

Combined P-I Diagrams for Flexure and Direct Shear

To quantify the response limits for both flexure and direct shear, pressure-impulse (P-I) diagrams are developed using the Single-Degree-of-Freedom Blast Effects Design Spreadsheet (SBEDS) (USACE 2008a). For the flexural mode, the SBEDS *Reinforced Concrete Beam or Beam-Column* component module is used to perform the SDOF analysis. Using SBEDS *General SDOF Program*, the SDOF analysis is performed for direct shear based on the resistance function described earlier. Since it is assumed that the member acts as a rigid body in this mode, all load mass factors are to be taken as unity. Since the direct shear slip will occur in the region of highest concentration of shear stresses, near the supports, the effective support rotation of the member can be evaluated at a distance, *d*, away from the supports where *d* is the distance from the top fiber of the member to the centroid of primary tension reinforcement. From this, effective support rotations can then be calculated based on each slip deformation level and used as the response limits when generating the direct shear *P-I* curves.

The *P-I* curves for both flexure and direct shear are combined into one plot as was previously done by Wei et al. (2013). To account for overlap in the *P-I* limits of flexure and direct shear a funneling technique, similar to work done by Low and Hao (2002), was used. As shown in Figure 5, once a direct shear *P-I* curve intersects a flexure curve, the flexural curve (lower capacity curve) controls the response and supersedes the direct shear curve. In this sense, the response limits for direct shear are treated as intermediate performance levels before the next flexural response limit is reached. The behavior of the curves in Figure 5 is in accordance with the outcomes of a study by Xu et al. (2014), which showed that direct shear behavior dominates in the impulsive loading region and flexural

behavior dominates in the quasi-static response region. This approach decouples the shear and flexural responses by presuming that no modifications caused by direct shear damage contribute to the flexural response. Further research is needed to assess the effect of the direct shear slip on the flexural stiffness of the columns, as the boundary conditions may be altered as a result of direct shear damage.

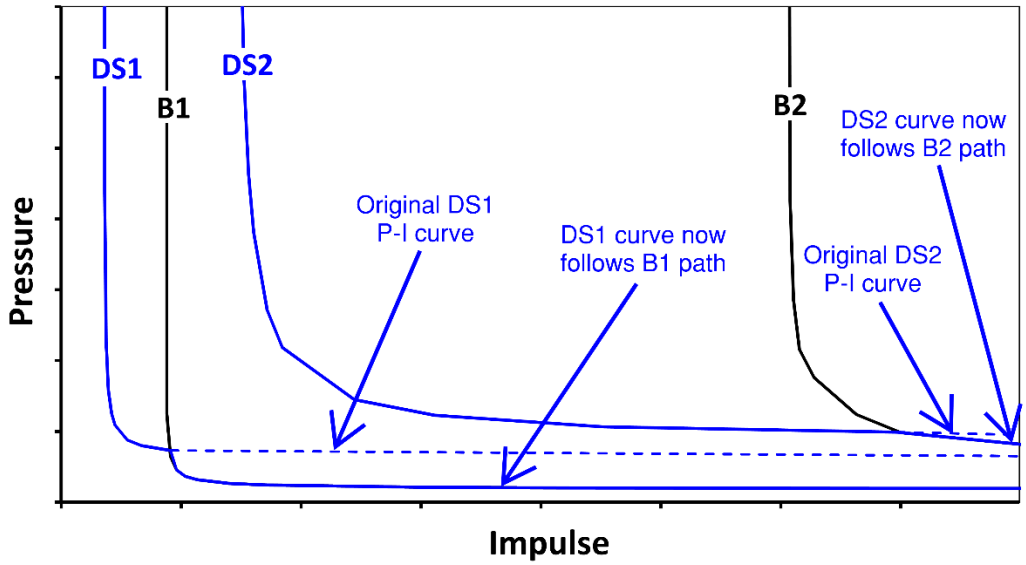

Figure 5 - Funneling of direct shear P-I curves ("DS") into flexural P-I curves ("B")

Step 3: Hazard Assessment

To ascertain the extent of blast-induced damage, the hazard consisting of an explosive charge weight and location must be determined. From this threat, incident and reflected pressure and impulse demands are computed on the exterior columns of the building. These values are determined at the base of each column (to evaluate breach) and at mid height (to evaluate flexure and direct shear) as illustrated in Figure 6. Flexural damage is evaluated at midspan since the lateral translation DOF is allowed at that location. Direct shear is also assessed at midspan since the shear stresses that develop in the column near its supports are caused by the rigid body motion of the entire member. Breach is

evaluated at the bottom of each column. This was done since the lower portion of each column is closest to the ground surface blast, breach is most likely to occur at that location. This theory is supported by a previous study by Osteraas (2006) which concluded that lower portions of perimeter columns should be designed, to the greatest extent possible, to resist the direct effects of blast.

To assess the demands on the column a tributary area of the façade must be considered. The tributary geometry is dependent on the relative strength, stiffness, and connectivity between the façade and column. Several possible tributary regions are illustrated in Figure 6. Type A assumes that the pressure wave is only exerted on the front face of the column and thus no contribution from the cladding is considered. Implementation of this area may be warranted in cases where the cladding system is assumed to be frangible. Type B assumes that the distribution to the horizontal and vertical elements is based on 45-degree yield lines. Type C represents a simplified conservative approximation of B and assumes that a portion of the cladding system (specifically closer to the column face) will maintain sufficient structural integrity to exert a blast-induced reaction force on the columns. Type D assumes a two way action between the vertical and horizontal framing elements with a larger contribution going to the columns. Type E represents a case where the facade is only attached to the vertical elements.

A mass tributary area, in addition to that used for pressure demand, must also be selected since a dynamic analysis will be performed on the column. The mass tributary area may be taken as the same as that used for pressure, or combinations of different types (A-E) may be used for mass and pressure. For example, a lightweight blast resistant cladding system (relative to the column mass) may warrant a larger pressure area relative

to that used for mass. Since this framework is designed to be compatible with any type of structure or cladding system configuration, the user may choose to implement the optimum tributary areas as they see fit for a specific case. The remainder of this study assumes that Types C and A are used for the pressure and mass, respectively. For Type C in this case, side dimensions of the tributary area are equal to the height of the column, h_{col} as shown in Equation (14). For corner columns, the tributary width is halved as depicted in Equation (15). Dimensions for Type A are that of the front face of the column.

Interior Columns: $$A_{trib} = {h_{col}}^2 \tag{14}$$

Corner Columns: $$A_{trib} = \frac{1}{2}{h_{col}}^2 \tag{15}$$

The incident pressure (P_{so}) at the critical points on the columns are computed relative to the threat using standard approaches of UFC 3-340-02 (DoD 2014) for hemispherical surface blasts of TNT. The incident pressure is computed from the scaled distance, Z in Equation (16), where R is the standoff distance in meters, and W is the mass of TNT in kg.

$$Z = \frac{R}{W^{\frac{1}{3}}} \tag{16}$$

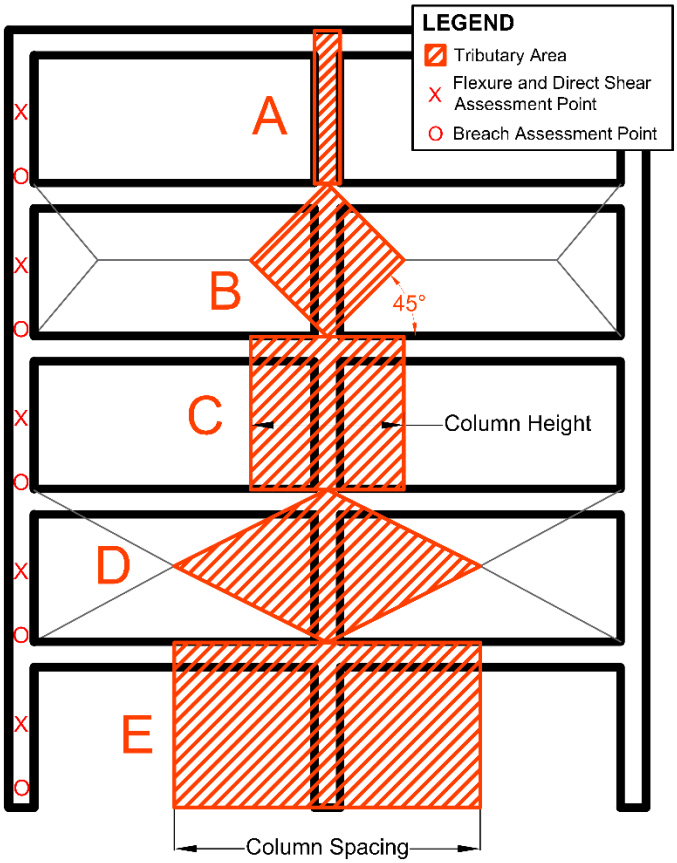

Figure 6 - Elevation view of a building frame showing possible column tributary area geometries (A-E) and damage assessment locations

The reflected pressure and reflected impulse are then calculated at each column by considering the orientation of the threat on the ground to each column. The angle of incidence between the explosive and each point on the building is used to account for reductions in the reflected pressure and impulse magnitudes. The angle of incidence can range anywhere between 0-90° with 0° implying a reflected pressure load applied normal to the building and 90° a side-on pressure equivalent to the incident pressure. UFC 3-340-02 defines the reflected coefficient, C_r, as the ratio of the reflected versus the incident pressure and is a function of the angle of incidence. A visual representation of angle of incidence geometry is shown in Figure 7 with an arbitrarily chosen x, y, z coordinate system

relative to the corner column base. The horizontal distance from the grid origin to the point of interest on the structure is x_i; *xBOMB* is the horizontal distance from the grid origin to the charge location; y_i is the vertical distance from the charge location to the point of interest; *yBOMB* is the vertical distance from the grid origin to the charge location; *Rg* is the standoff distance normal to the building face; and *Rspace* is the direct distance from the charge location to the point of interest on the building and is used for calculating the standoff.

In this model, two angles of incidence are considered. The first, labeled α in Figure 7 and calculated using Equation (17), accounts for both the horizontal and vertical reflected angle, combined into one angle in space. The angle α is used for evaluation of the flexure and direct shear modes discussed later in the paper. The second angle, α' (Equation (18)), is used when analyzing the breach failure mode and only considers the vertical reflected angle. Unlike flexure and shear, breach behavior is not dependent on the orientation of a specific geometric axis but rather the gross cross section of the column. Consequently a conservative approach is made to assess the breach hazard relative to only the vertical angle of incidence. The two angles are used to develop two separate distributions of reflected pressure and impulse on the building surface.

$$\alpha = \tan^{-1} \frac{\sqrt{|x_i - xBOMB|^2 + |y_i - yBOMB|^2}}{Rg} \tag{17}$$

$$\alpha' = \tan^{-1} \frac{|y_i - yBOMB|}{\sqrt{Rg^2 + |x_i - xBOMB|^2}} \tag{18}$$

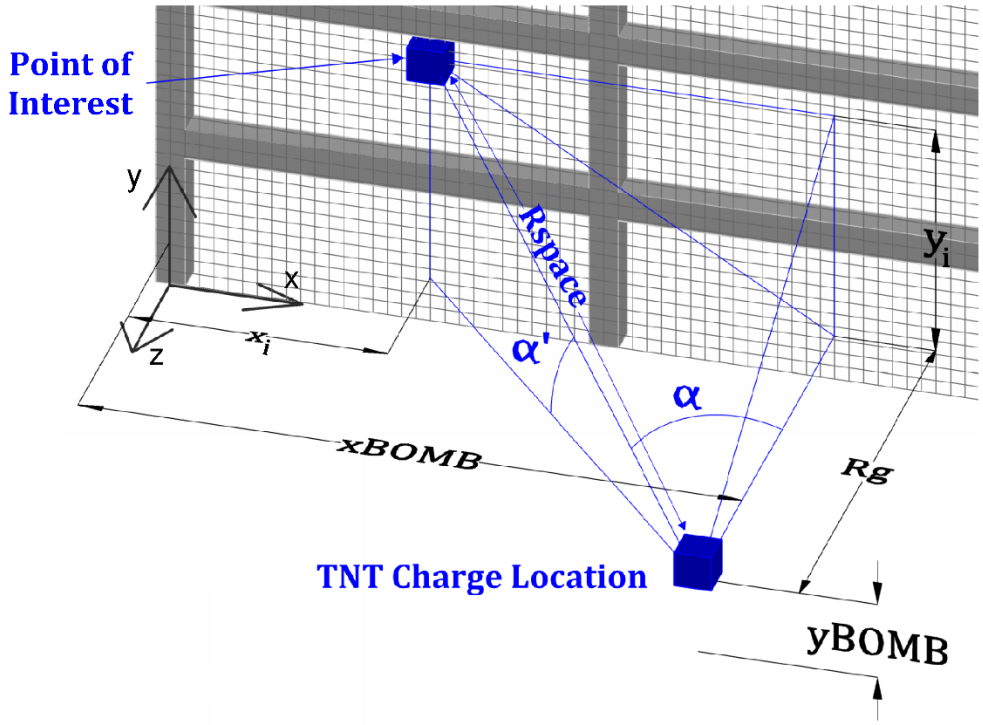

Figure 7 - Geometry relative to building surface for calculation of angle of incidence

Step 4: Damage Assessment

The occurrence of breach is assessed first for each column by comparing the P_r and I_r measured at the bottom of each column to the breach capacity of that column. If the capacity is exceeded, then the column is designated as breached and effectively "removed" from contributing to the performance of the frame. If breach does not occur, the column is evaluated for flexure and direct shear by comparing the combined *P-I* capacity curves with the P_r and I_r measured at the mid-height of each column. The damage level of each column is then determined based on its response level, and the contour of all column damage is plotted to show the extent and severity of damage. This process can be repeated for a series of blast threats (i.e. for a range of charge weights at varying standoffs) to obtain an envelope of the damage distribution. A numerical example for developing an envelope is provided in the following case study.

Step 5: Quantification of Structure Robustness

After the spatial distribution of column damage has been determined, the structure can then be evaluated for resistance to progressive collapse. For each damage scenario, a robustness index for the building can be calculated. The robustness measures the collapse resistance of the building relative to both the loads for which it was designed as well as its undamaged capacity. Using this simplified approach, the level of load at which the structure collapses can be conveniently assessed based on its characteristics and required loading demand.

The first step in calculating the robustness of the building is to impart the deflection corresponding to the appropriate damage level at each column as an out-of-plane displacement. Although the column deformations resulting from both flexural and direct shear demands are measured, each initial column out-of-plane displacement will be rounded up to the next flexural response limit as a conservative estimate. Future studies will consider the effect of direct shear deformations on the flexural capacity of the section.

To assess the in-plane behavior of a damaged moment frame building, the out-of-plane deformations are used to calculate the resulting out-of-plane P-Delta moment on each column. This moment, M, will be calculated using Equation (19) where P is the axial load in the column of interest and Δ is the blast-induced out-of-plane displacement at each column. The P-Delta moment is used to determine the residual in-plane moment-axial force interaction curve of each column. This is done by first generating the interaction surface of axial load and biaxial bending (i.e. PMM surface) for each column type. The 3D surface can then be sliced at the corresponding value of P-Delta along the out-of-plane axis leaving

the in-plane axial-moment interaction curve. An example of the interaction surface slicing is detailed later in the paper.

To assess the behavior of the damaged structure, a 2D finite element model can be generated. A nonlinear pseudo-dynamic analysis is used to determine the maximum response of the damaged building to increasing levels of dead and live floor loads. A uniform pushdown method of load application is recommended for this framework where the factored dead and live floor loads are amplified by a factor, γ as shown in Equation (20) where DL and LL are the unfactored dead and live floor loads, respectively, until collapse ensues. It is assumed that during the blast loading, all beams were restrained against out-of-plane bending due to their connection to the floor diaphragm.

$$M = P \times \Delta \tag{19}$$

$$Total\ Floor\ Load = \gamma(1.2DL + 0.5LL) \tag{20}$$

The nonlinear pseudo-dynamic analysis approach involves the definition of plastic hinge properties for all columns and beams within the structure. For the columns, the moment and axial force in the member is compared with its in-plane axial-moment interaction curve. The column hinge forms once its response reaches the interaction capacity curve. For the beams, moment capacity is plotted against the end rotation of the member. Input parameters for the plot are defined and quantified in ASCE (2007) and are a function of the cross-section properties of the member. Acceptance criteria is also defined as three levels of hinge rotation, each representing a level of damage to the structure. These criteria and their qualitative definitions are shown in Table 3below. For this framework,

the structure as a whole is deemed to have collapsed when the first collapse prevention (CP) hinge forms in a beam within the frame. It is important to note that when comparing the relative severity of several different damage scenarios that consistent acceptance criteria and collapse mechanisms be used throughout.

Table 3 - Moment-rotation response acceptance criteria

Acceptance Criterion	**Acronym**	**Description**
Immediate Occupancy	IO	Maximum allowable rotation to allow for immediate occupancy of building following damage event.
Life Safety	LS	Maximum allowable rotation to provide adequate protection against occupants in building.
Collapse Prevention	CP	Rotation level at which collapse of the member will ensue following a damage event.

To quantify the resistance of the structure to progressive collapse following the exposure of blast-induced loads, a relative robustness index (RRI) approach developed by Fallon et al (2016) was adopted for this framework. In this approach, uniform floor load pushdown is used to calculate the progressive collapse resistance of a damaged building relative to its undamaged state under its intended design loads. The RRI number for a given building can be determined by first performing the uniform pushdown on an undamaged building simply by amplifying its design loads until collapse (i.e. the formation of a CP hinge in a beam) is reached. The floor load amplification factor at collapse, noted as $\lambda_{undamaged}$, is then recorded. It should be noted that a dynamic increase factor for the loading was not used in this study. This was to maintain consistency in calculating the robustness index between damage scenarios with and without column removals. Future phases of this

study will explore the effect of the dynamic increase factor on the collapse mechanisms for this type of analysis. The uniform floor load pushdown procedure is then repeated for the damaged structure until it experiences collapse, and its corresponding amplification factor is recorded as $\lambda_{damaged}$. The resulting RRI for the damaged structure can then be calculated using Equation (21). The value of RRI for a given building and damage scenario can then be compared with the same building exposed to a different damage scenario to assess their relative consequences.

$$RRI = \frac{\lambda_{damaged} - 1}{\lambda_{undamaged} - 1} \tag{21}$$

CASE STUDY: 10-STORY REINFORCED CONCRETE BUILDING FRAME

A prototype reinforced concrete framed office building, based on that used in a previous study by Lew et al. (2011), is used to demonstrate the applicability of the proposed framework. Steps 1 through 4 of the proposed framework shown in Figure 2 are implemented to evaluate the extent of damage caused by a range of blast threats.

Case Study Step 1: Design

The building was designed with intermediate moment frames for conventional loads and for seismic loads in accordance with Seismic Design Category (SDC) C (ASCE 2010; ICC 2012). The long dimension exterior frame, consisting of 10 stories with a total height of 37.49 m (123 ft), is examined this case study. A front face elevation view is shown in Figure 8a. All columns were spaced 9.14 m (30 ft) on center and two column heights were used: a ground to first floor height of 4.57 m (15 ft) and all story heights above equal to 3.66 m (12 ft). Normal weight concrete with a unit weight of 23.6 kN/m^3 (150 lb/ft^3) and a nominal compressive strength of 27.6 MPa (4000 psi) was specified. All columns in the

frame have the same reinforcement and cross-section and are reinforced with sixteen #32 Grade 420 (#10 Grade 60) bars as shown in Figure 8b. A dynamic increase factor of 1.19 and 1.17 is used for concrete compressive strength and rebar yield strength, respectively, to account for material strengthening at high strain rates.

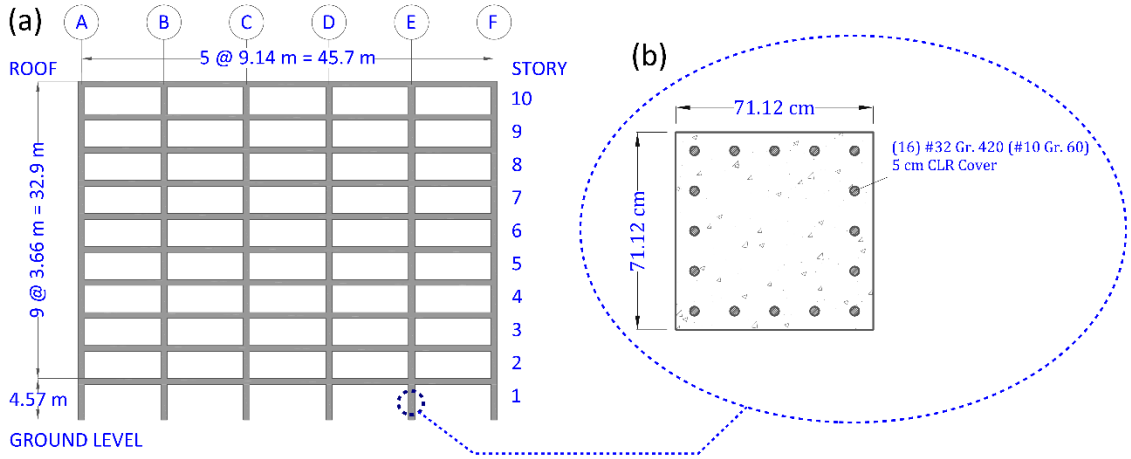

Figure 8 - Prototype RC building frame: (a) front face elevation and (b) typical column section details

Case Study Step 2: Capacity Assessment

The breach threshold curves for the prototype columns calculated using Equations (1)-(3), are shown in Figure 9. The flexural resistance functions are obtained using standard resistance calculations for reinforced concrete (DoD 2014). The effect of axial load is included based on the *P-M* interaction diagram. Consequently, as axial force increases in descending stories due to cumulative tributary floor loads, the magnitude of the flexural resistance increases. This effect is illustrated by comparison of the flexural resistance of the interior and corner 2nd and 10th story columns in Figure 10. Based on the column geometry and material properties, the response limits for direct shear were calculated using Equations (5) through (11). The calculated shear resistance, R_{DSi}, without the consideration

of applied axial load at each critical level of direct shear slip, Δ_{DSi}, is shown in Table 4. When the axial load is included, the shear strength is magnified to a value R'_{DSi}. The increase in strength as a function of story number is shown in Figure 11. It is conservatively assumed that the deformation limits do not change as a function of axial loading.

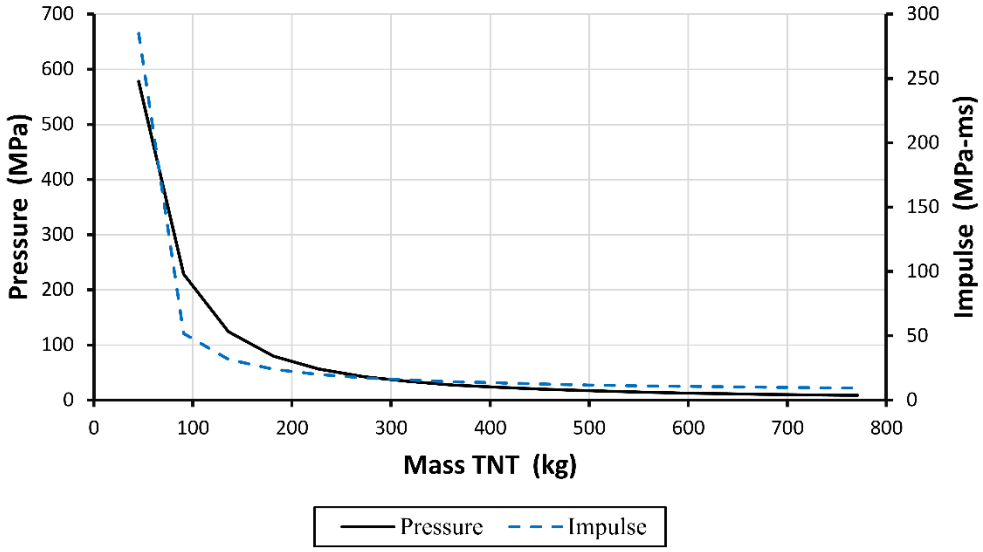

Figure 9 - Breach threshold curves for prototype building column

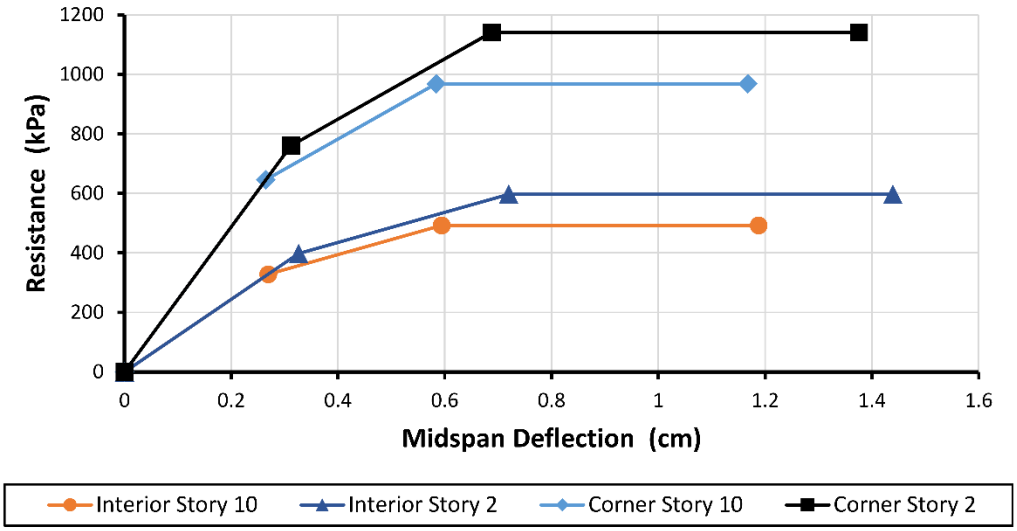

Figure 10 - Flexural resistance functions for corner and interior columns on floors 2 and 10

Table 4. Direct shear response limits without consideration of applied axial load

Response Label	R_{DSi} (MPa)	Δ_{DSi} (mm)
DS1	1.158	0.11
DS2	2.044	0.30
DS3	2.044	0.61
DS4	1.447	3.51
DS5	1.447	115

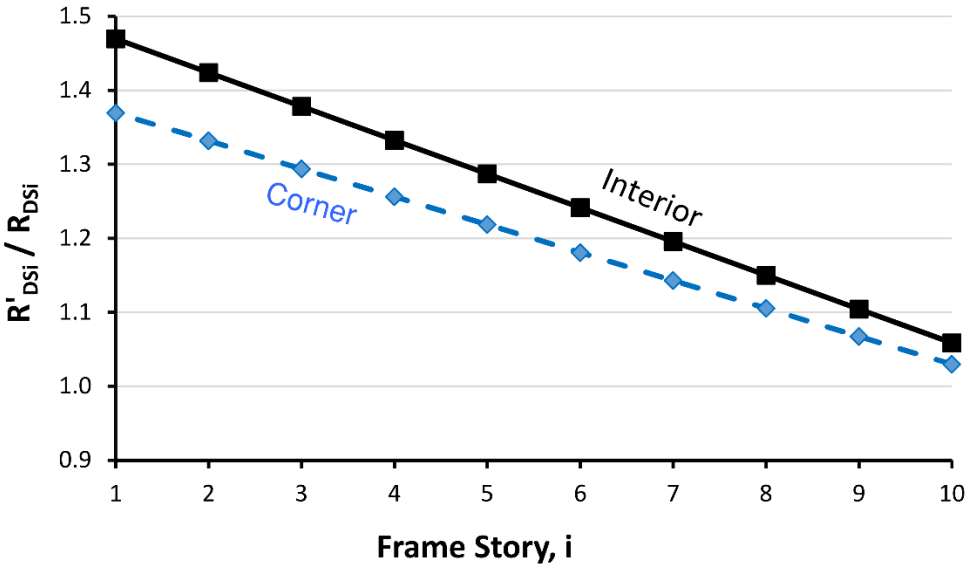

Figure 11 - Axial load magnification factor for direct shear resistance as a function of frame story

The flexural *P-I* capacity diagrams are determined for interior and exterior columns at each story. Tributary areas for interior and corner columns were calculated using Equations (14) and (15), respectively. Boundary conditions are assumed to be fixed-simple for this example. This set of boundary conditions was chosen as an approximation of resistance that falls between two extrema: simple-simple as an upper bound and fixed-fixed as a lower bound for estimating deflections (and vice versa for estimating shear reactions). Alternate boundary conditions could be used based on the detailing of the system. All

column types were analyzed as undamped, and both initial displacements and velocities were set equal to zero. The resistance functions for flexure (shown in Figure 10) and direct shear (as depicted in Figure 4 using parameters from Table 4 and Figure 11) for corner and interior columns at each story were used to develop *P-I* capacity curves. A total of twenty sets of *P-I* capacity curves were generated to capture the variety of column heights, axial loads and tributary areas in the building. Four of the *P-I* diagrams are shown for comparison in Figure 12: (a) interior column, story 2; (b) interior column, story 10; (c) corner column, story 2(c); and (d) corner column, story 10.

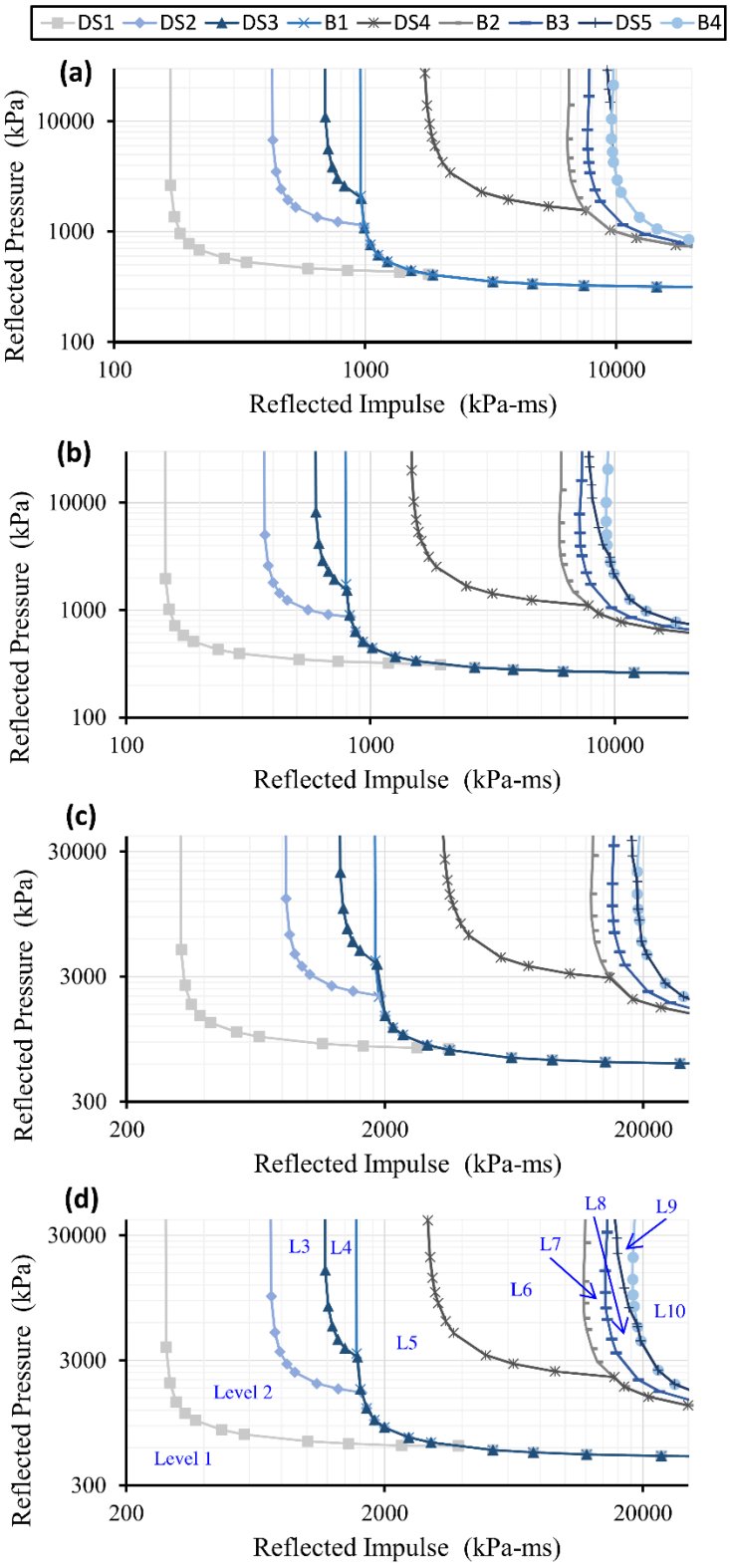

Figure 12 - Combined flexure and direct shear P-I diagrams: (a) interior story 2, (b) interior story 10, (c) corner story 2, and (d) corner story 10

Case Study Step 3: Hazard Assessment

For this case study two hazard scenarios are examined. In scenario A, the threat size and location are both known. In scenario B, the threat size is known but the location varies over a pre-defined region at ground level near the building's perimeter.

Hazard scenario A consists of three hazards of increasing charge size: DL1 through DL3. The size and location of the charges were chosen to demonstrate the different levels of damage that could occur over the building frame. The TNT charge weight (*W*), standoff distance (*Rg*), and x-axis coordinate of charge location (*xBOMB*) corresponding to the three demand levels are summarized in Table 5. All charges are assumed to be placed on the ground (thus *yBOMB* is equal to zero). DL1 and DL2 charges were placed (along the x-axis) directly normal to the center of the column face. DL3 was placed halfway between column lines. In practice, these threats would be specified by the owner, the governing standard, or the results of a threat assessment. The location of the threat would be assessed relative to the site layout and the available standoff based on obstructions or operational security.

Table 5. Trial TNT charge weights and standoffs corresponding to building frame damage levels

Building Damage Level	No. of Columns Removed	TNT Charge Wt., W (kg)	Standoff Distance, Rg (m)	xBOMB (m)
DL1	0	226.8	3.05	18.29
DL2	1	453.6	3.05	18.29
DL3	2	907.2	6.10	13.72

The reflected pressure and impulse demands for the three scenario A charges were determined using the approach previously discussed. For illustration purposes, the *P-I* blast

demand values are shown as contours over the entire surface of the building from which the damage at discrete locations can be assessed. For the proposed threat dependent assessment, these values are only needed at the mid-height of the column and at the column base. The reflected pressure and impulse are plotted as contours for each hazard for the flexure and direct shear assessments in Figure 13. Recall that different *P-I* measurement locations are used for the breach and flexure/direct shear assessments. The breach hazard contours for the case of DL3 is illustrated in Figure 14. The horizontal and vertical lines represent the framing of the structure and the squares represent the locations on each column where the damage assessment is made. Comparing the DL3 hazard for breach and flexure/shear it is evident that utilizing just the vertical angle of incidence for the case of breach provides a conservative estimate of the hazard.

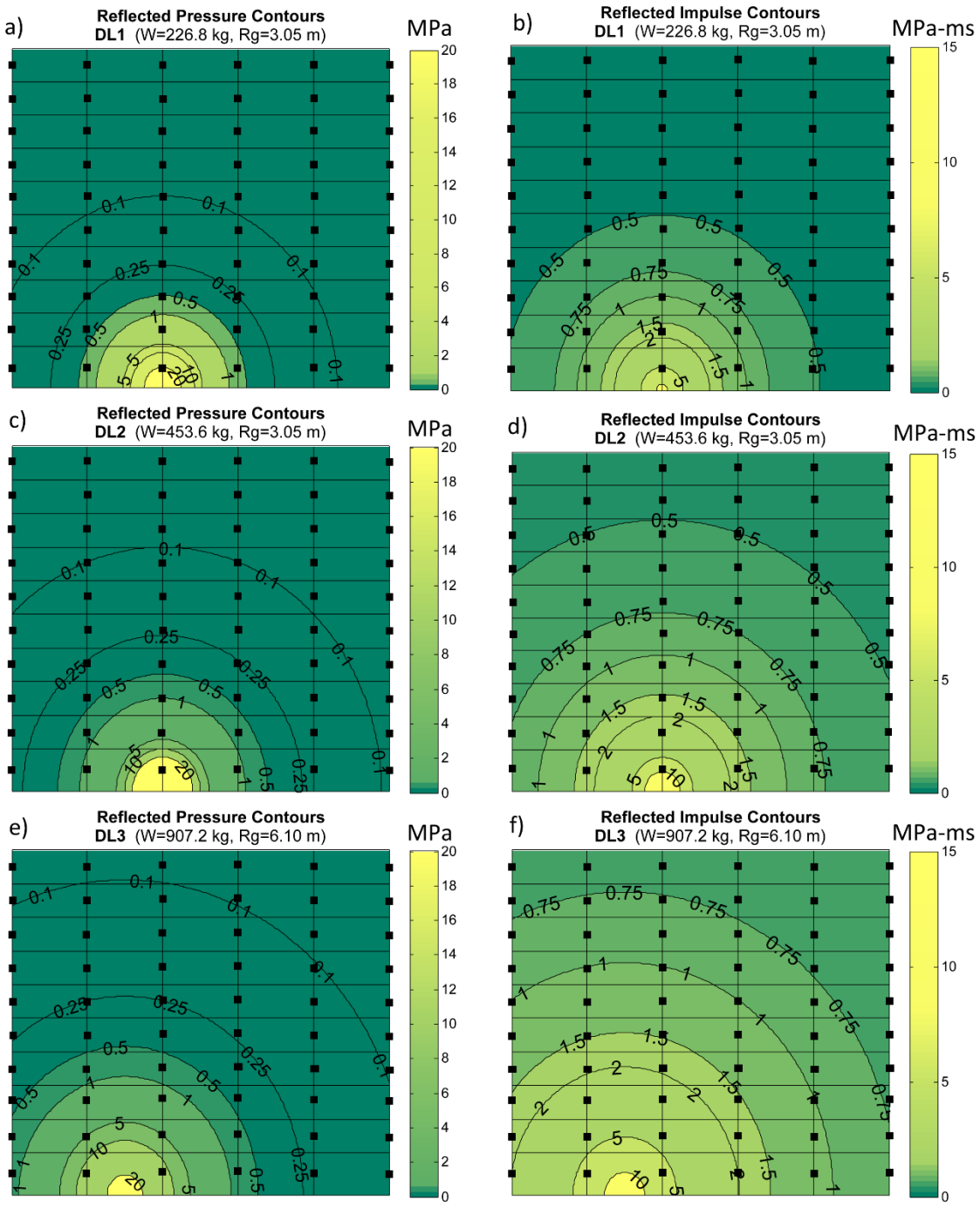

Figure 13 - Reflected pressure and impulse contours for flexure and direct shear modes plotted on building surface for the three threat scenarios

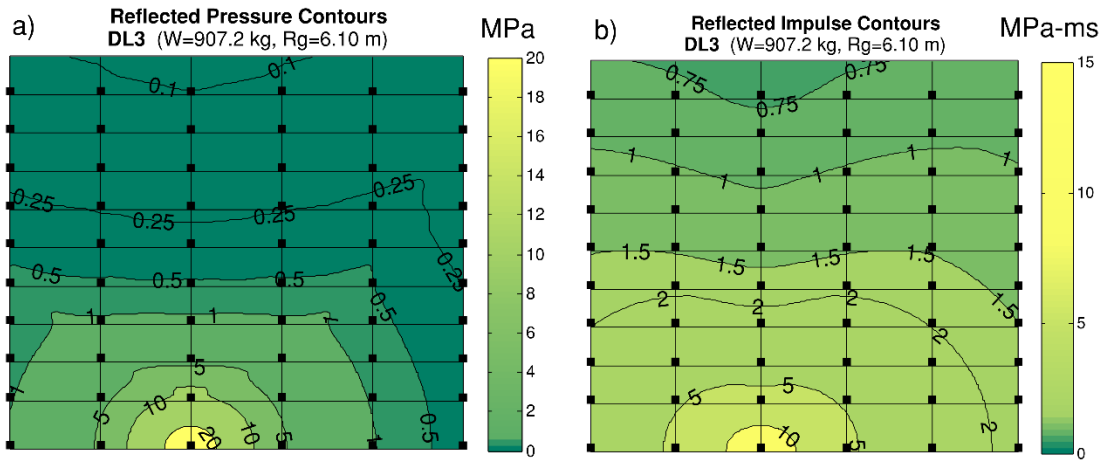

Figure 14 - Reflected pressure and impulse contours for breach plotted on building surface for the DL3 threat scenario

Hazard scenario B consists of three conventional charge sizes. This includes an 11.34 kg (25 lb.) satchel size explosive, a 99.79 kg (220 lb.) small vehicle borne improvised explosive device (S-VBIED), and a larger VBIED (L-VBIED) 907.2 kg (2000 lb.) bomb. In this set of trials, each of the charges was located on the ground over a region in front of the structure. The region of threat is assumed to be bounded by the corner of the building and center of the building face and standoff distances ranging from 3.05 to 24.4 m (10 to 80 ft.) as illustrated in Figure 15. For this case study the assumption is made that a protected space exists 3.05 m (10ft) from the face of the building. The 24.4 m (80 ft) extent was selected based on recommended design criteria from UFC 4-010-01 (DoD 2013a), which denotes that tradeoffs between standoff distance and building component construction will generally need to be analyzed when standoff distances are less than 25 m (82 ft.). The demand on the first floor columns were determined for each charge located at points distributed at 0.3 m (1ft) spacing over the threat region.

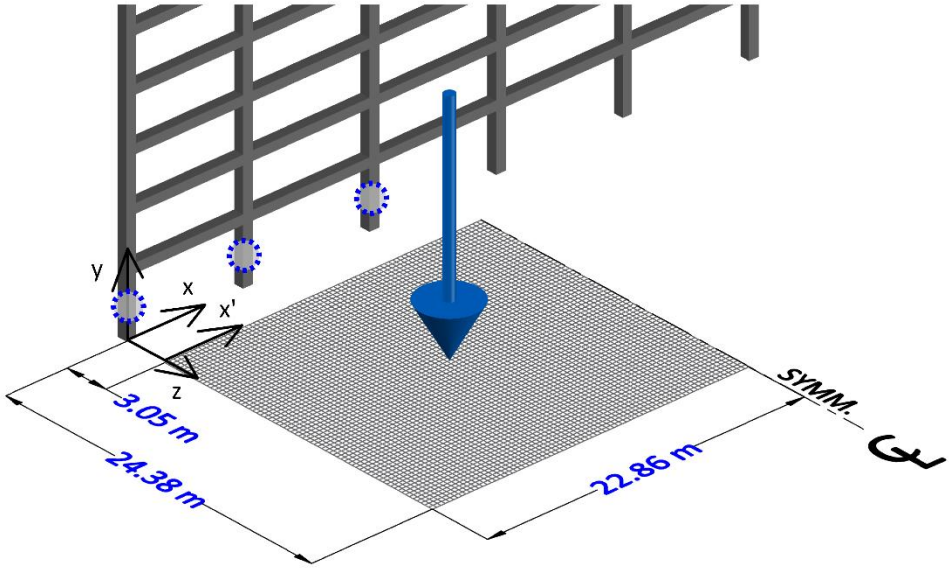

Figure 15 - Isometric view of prototype building frame showing grid used for generating standoff contours for first floor column damage

Case Study Step 4: Damage Assessment

Damage is assessed for the two hazard scenarios: (1) damage on the building for a given threat size at a given location, and (2) damage on the first floor columns for a given threat size at various locations in front of the building. The first hazard scenario is used to illustrate the extent of damage that can occur to columns over the height of the building. The second hazard scenario is used to illustrate the standoff distances needed to prevent multiple column damage. Damage levels for the two scenarios and threat sizes and locations are determined by comparing the blast-induced pressure and impulse values to the respective *P-I* capacity curves for each column.

Hazard Scenario A: Known Threat Location

The resulting damage states for all columns for each hazard are mapped onto the building. The analysis is conducted first by considering axial demands on the flexural response of the columns and again by neglecting axial effects. As mentioned earlier, for

the prototype reinforced concrete columns, the axial force will increase the flexural strength but may decrease the resistance as *P-Δ* effects become significant due to large deflections. A comparison of these cases can be used to examine the sensitivity of axial effects on the damage distribution through the structure.

To simplify the illustration of damage on the building frame, the breach/flexure/direct shear response limits are combined to develop a comprehensive damage scale ranging from level 1 to 11. The levels are chosen to represent the regions between the *P-I* capacity curves (see Figure 12d). Level 1 corresponds to minimal damage while level 11 corresponds to breach of the column. As shown in Figure 12, the shear modes control the lower damage levels followed by an intermixing of shear and flexure response levels and ending with breach. The damage levels 1 through 11 are summarized in the legend of Figure 16 relative to the flexure, direct shear, and breach response limits. The levels were chosen based on increasing impulse and pressure and are specific to the system under investigation. The damage level maps for the case study are illustrated on the building frame in Figure 16.

The hazard scenario A resulted in distribution of damage over multiple columns on the building face. The overall damage increases with the increasing hazard levels (DL1, DL2, and DL3). Hazard DL1 results in damage level 8 in one column and level 5 in adjacent columns when axial load is considered. This correlates to high flexural and shear damage in the first floor column and moderate shear and low flexural damage to all the adjacent columns. Each hazard results in damage to multiple columns. This is in contrast to the APM which notionally removes one column and assumes all other columns are undamaged. This spread of damage to multiple columns within a frame could potentially

compromise its structural integrity. Similar damage distribution occurs for the other hazard cases. DL2 results in breach of one column and moderate damage to adjacent members. DL3 results in breach of two adjacent columns and moderate damage over a large region of the building face. These results indicate that a threat dependent damage assessment may be warranted for moderate blast loads.

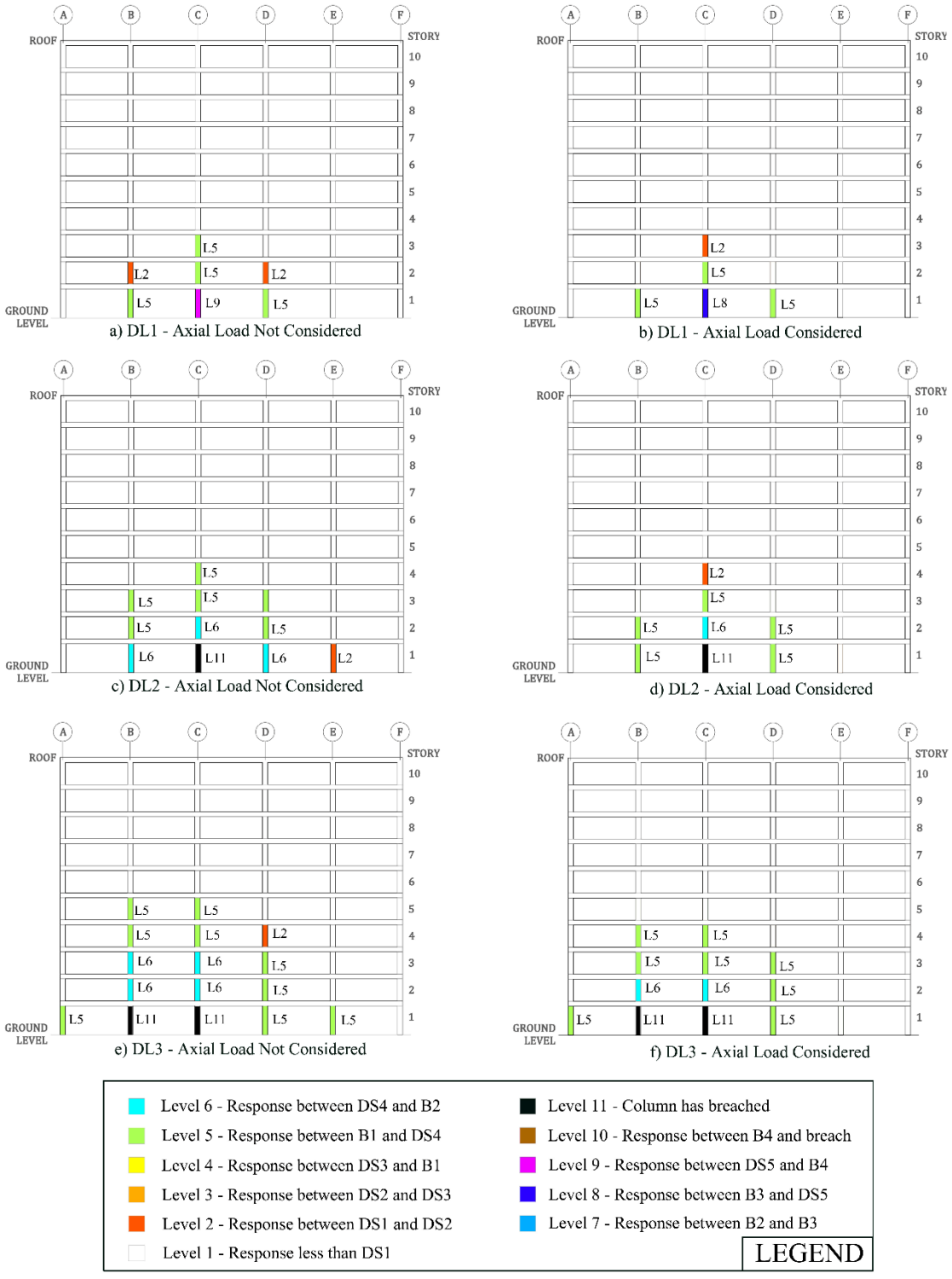

Figure 16 - Building frame damage map

In this study, accounting for axial load effects on the columns improves the damage resistance of the frame when subjected to blast demands. Figure 16 compares the level of

damage to the columns when axial effects are included and when they are not for the three demand levels DL1, DL2 and DL3 (compare (a) to (b), (c) to (d), and (e) to (f)). The inclusion of axial effects reduces both the spread and level of damage over the face of the building. This effect is clearly illustrated in the reduction of first floor column damage under the DL2.

Hazard Scenario B: Variable Threat Location

For cases where the specific threat location is not known, a damage assessment can be conducted over a region of potential charge locations. The damage generated by the three aforementioned charge sizes was determined at numerous locations within a region near the building perimeter. The satchel size was used to assess the vulnerability of the structure to a very close-in demand, potentially detonating near the lower portion of a critical column. The S-VBIED is useful for simulating more widespread pressure and impulse demands on the face of the building from a larger standoff distance. The L-VBIED was implemented to assess the vulnerability of the structure to large pressure and impulse demands and was used to assess the state of the structure when suffering significant, widespread structural damage.

The damage states for the first floor columns were determined for each charge size based on the varying standoff distances. These standoff contours are illustrated in Figure 17 for the three charge sizes: (a) L-VBIED, (b) S-VBIED, and (c) satchel charge relative to the positions of the first floor columns on lines A, B, and C. The arrow shown in Figure 15 shows the view perspective for the plots of Figure 17. The contours in Figure 17 are only plotted on half the ground surface grid since the building is symmetrical (thus the

contours for columns on lines D, E, and F will be the same as those for columns on lines C, B, and A, respectively).

The results of these trials illustrate the relationship between charge location and multiple column damage. For the case study structure, the columns subjected to the satchel type explosive are limited to level 3 damage (see Figure 17c), and damage occurs only for close-in locations. Due to the small size of the explosive, no threat location produces damage to more than one column at a time. As the charge size is increased to that of the S-VBIED, damage to multiple columns can occur for a range of charge locations. For example, if the S-VBIED is placed at the location of the star in Figure 17b, first floor columns on lines A, B, and C would experience damage levels of 1, 5, and 2, respectively. The column damage interaction becomes very pronounced for the L-VBIED, for which specific locations can result in breaching (and thus removal) of two columns along with significant damage to other adjacent columns (see Figure 17a).

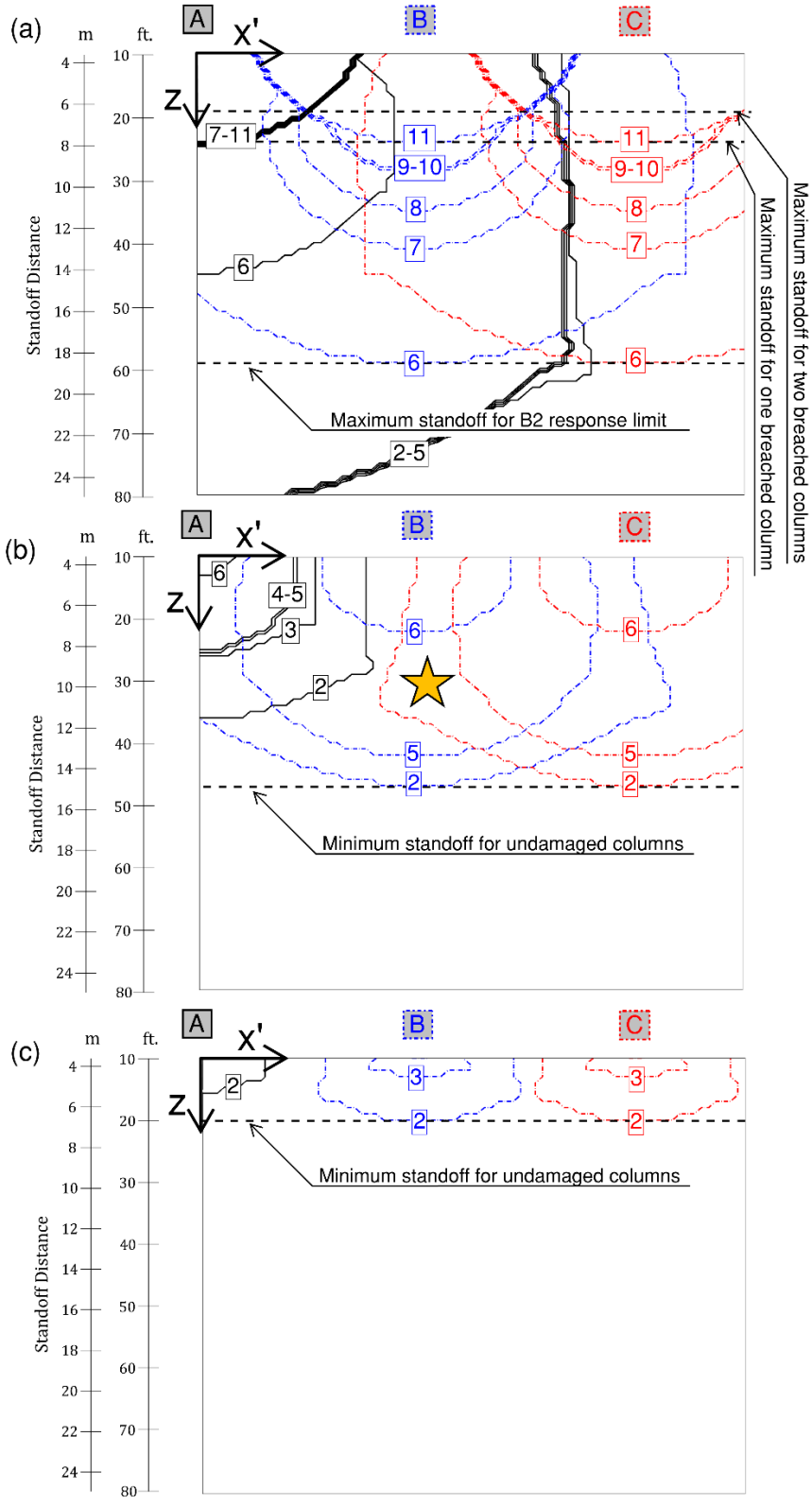

Figure 17 - Plan views of standoff contours for first floor column damage levels for three charge sizes: (a) L-VBIED, (b) S-VBIED, and (c) satchel

These damage contours are used to develop standoff distance boundaries for critical response limits. The minimum standoff distance for all columns in the frame to remain undamaged, i.e. below the DS1 limit state, is 6.10 m (20.0 ft.) and 14.38 m (47.19 ft.) for the satchel and S-VBIED charge sizes, respectively. For the L-VBIED charge size, the maximum standoff distances are 18.03 m (59.14 ft.), 7.25 m (23.79 ft.), and 5.73 m (18.79 ft.) for B2 response limit, breaching of only one column, and breaching of two columns, respectively. The ground surface contours create damage level envelopes that can be used in the preliminary design phase of the building to assess the risk of damage for a given standoff distance or for existing structures to determine recommended locations for secured standoff fences.

Case Study Step 5: Quantification of Structure Robustness

In order to quantify the effects of the threat-dependent damage scenarios on the collapse resistance of the prototype building frame, a nonlinear pseudo-dynamic progressive collapse analysis was performed using SAP2000 (CSI 2014). The pseudo-dynamic approach allows the user to slowly amplify the gravity floor loads as a function of time in order to monitor the development of hinge mechanisms and capture the amplification factor at the collapse load. To simulate the static loading case, the load was applied over a very long time period in order to eliminate any sort of vibration response of the structure. As mentioned earlier, collapse of the frame was dictated by the development of the first collapse prevention (CP) hinge in a beam.

The exterior beams in the prototype structure and adopted from Lew et al (2011) have dimensions of 71.1 cm (28 in.) in width and 50.8 cm (28in) in depth. The end zones of the beam (i.e., the negative moment region) consist of (9) #29 Gr. 420 (#9 Gr. 60) bars

at the top (tension steel) and (3) #29 Gr. 420 bars at the bottom (compression steel). Stirrups consist of two legs of #13 Gr. 420 (#4 Gr. 60) bars spaced 10.2 cm (4 in.) on center up to 106.7 cm (42 in.) away from the column face. Since the concrete in the structure is monolithic, the beams exhibit a compressive strength of 27.6 MPa (4000 psi) as seen also in the columns. A schematic of the beam end zone geometry and reinforcement detailing is shown in Figure 18 below.

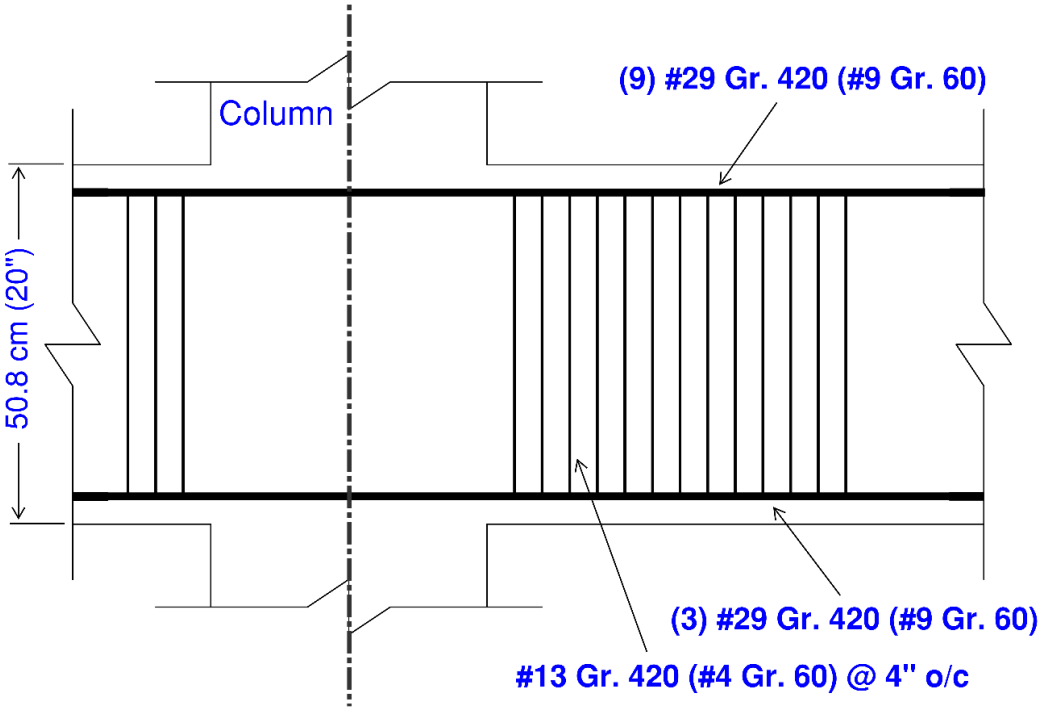

Figure 18 - Typical prototype building frame moment connection details

To develop the moment-rotation relationships for the beam end zone hinges, the cross-section properties were used to select the parameters *a*, *b*, and *c* and acceptance criteria from ASCE (2007). Figure 19 shows the moment-rotation plots for the given beam section with the acceptance criteria defined in Table 3 also shown on the curve. The evaluation of column overloading was also performed using the assignment of hinges in the column end zone regions. The column hinges were defined using the residual in-plane

moment-axial force interaction curve resulting from the slice of the three dimensional axial force and biaxial moment (PMM) interaction surface. To generate the surface, a two dimensional fiber section analysis model was developed. The column cross section was discretized into 256 square fibers, 28 along each edge, with side dimensions all equal to 2.54 cm (1 in.) as shown in Figure 20. Each point of the PMM curve corresponds to a given neutral axis depth, *c*, and angle of rotation, θ, as depicted in Figure 20. The three dimensional PMM surface generated for the columns in the prototype structure is shown in Figure 21. The PMM surface was then sliced at the appropriate out-of-plane P-Delta moment resulting from the blast damage, thereby producing the residual in-plane PM interaction curve for each column at its respective damage level.

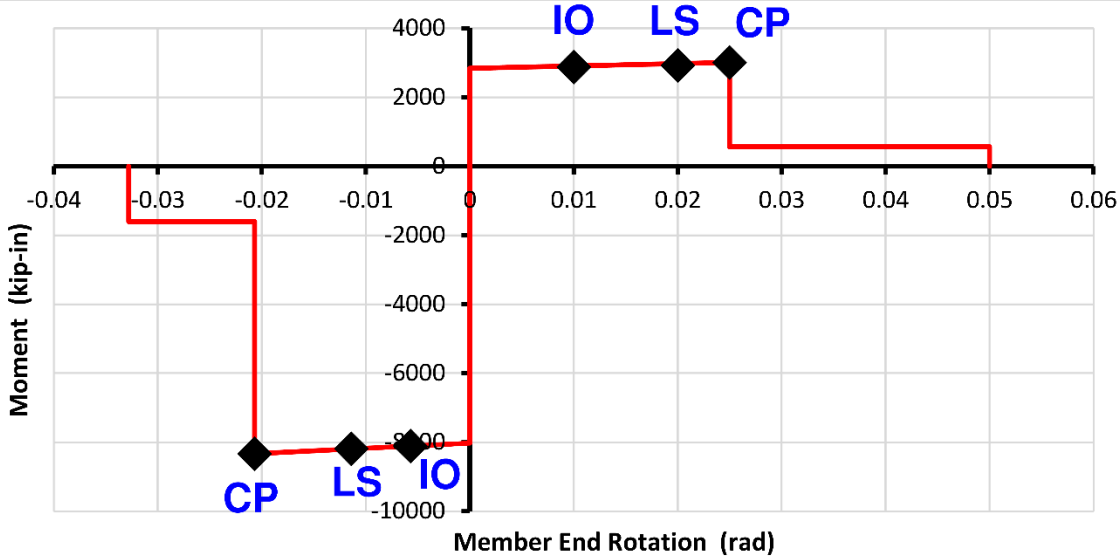

Figure 19 - Moment rotation modeling curve and acceptance criteria

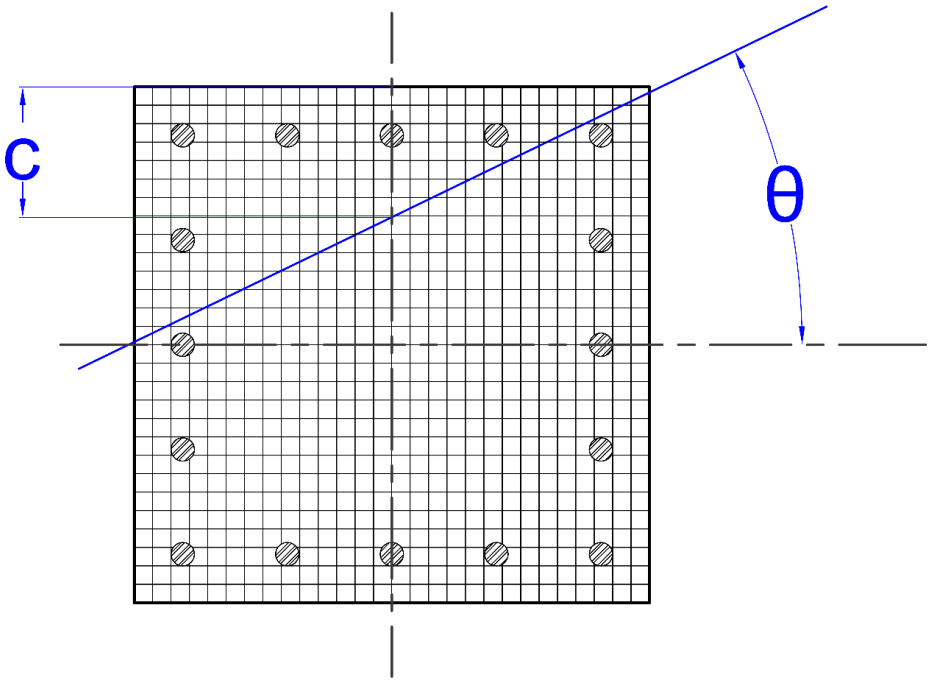

Figure 20 - Column represented as a two dimensional cube fiber section

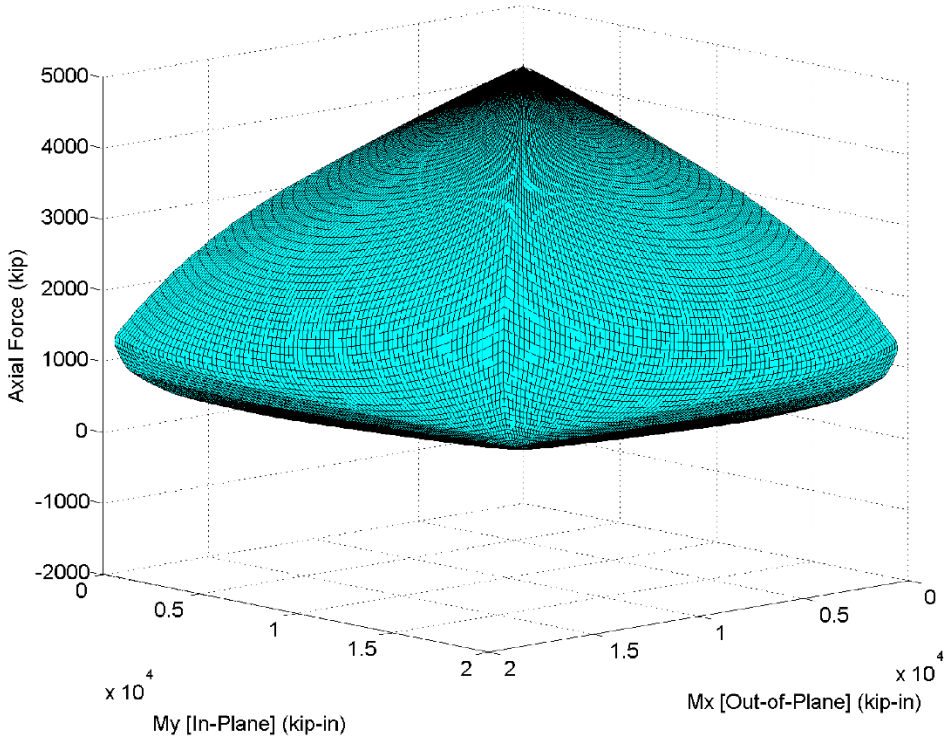

Figure 21 - Three dimensional PMM surface for columns in prototype frame

Four different damage scenarios of the prototype building were compared in this case study. The full, undamaged structure with no column removals, was used as the control for calculating the RRI for the damage states. The second scenario was the structure exposed to the DL1 damage map (see Figure 16b) created in *Hazard Scenario A* of *Step 4*. The third entailed the notional single column removal without any damage to adjacent columns. And finally, the fourth scenario involved the structure being subjected to the DL2 damage map (see Figure 16d). The condition DL3 (see Figure 16f), where the blast load resulted in the removal of two columns, was not considered in the robustness calculations as the stability of the structure would not be achievable at the onset of the uniform pushdown analysis. It should be noted, however, that the DL3 scenario is achievable for a range of large threat sizes and may be warranted for consideration when planning the design of the building and its surrounding site layouts. This scenario can potentially be mitigated by increasing standoff distances or by strengthening the columns as needed.

A comparison of the reduced in-plane moment-axial force interaction curves for the prototype column at the three levels of damage is shown in Figure 22. Columns with L8 and L5 damage result from the DL1 scenario as shown in Figure 16b and columns with L5 and L6 damage levels are present in the DL2 case as seen in Figure 16d. Recall that L11 damage is considered as a removal for the DL2 scenario. Also, the L2 damage levels mapped on column line C in Figure 16b and d were not considered for the pushdown analysis since they represented only a small amount of direct shear slip near the column supports. Further research by the author will investigate the effects of direct shear deformations on the residual axial capacity of the columns. These reduced curves were then used as input for the column hinges in the nonlinear pseudo-dynamic model.

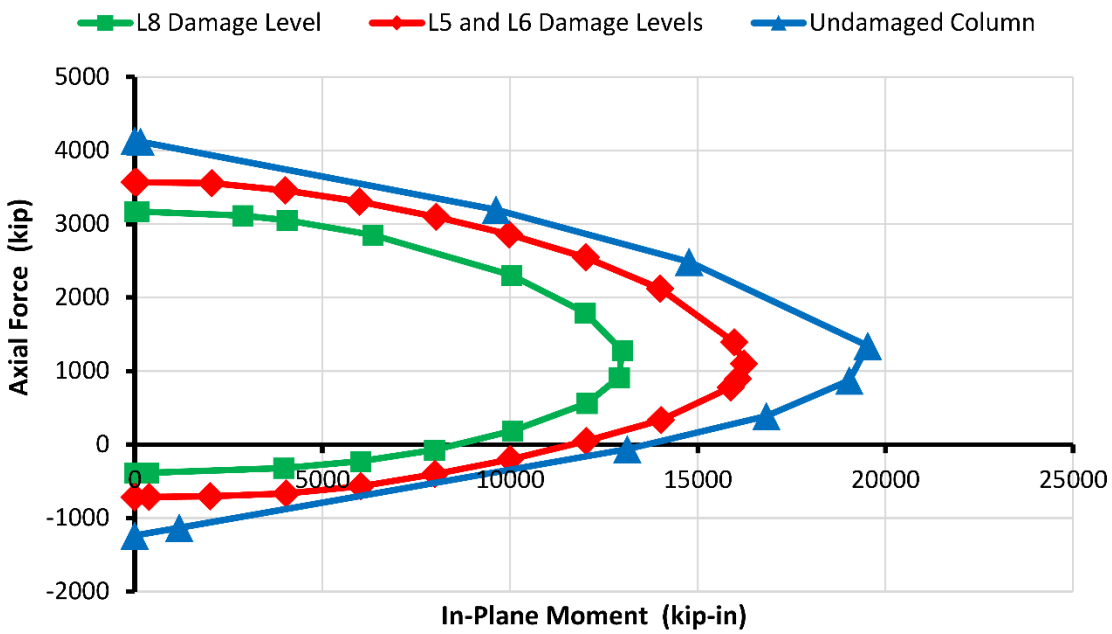

Figure 22 - Comparison of reduced in-plane moment-axial force interaction curves for the prototype column for three damage cases

After performing a uniform floor load pushdown for all four damage scenarios, the RRI values for each case were calculated and compared with one another. The undamaged building frame saw the development of its first CP beam hinge at a floor load amplification factor ($\lambda_{undamaged}$) equal to 5.55. This results in a baseline RRI of 1 for the undamaged structure following the approach presented by Fallon et al (2016). The DL1 damage scenario collapsed at a floor load amplification factor ($\lambda_{damaged}$) equal to 4.31 and comparing to the value of $\lambda_{undamaged}$ yields a RRI of 0.726 for that case. The notional single column removal case developed a CP beam hinge at a value of $\lambda_{damaged}$ equal to 0.896 resulting in a RRI of -0.023. Finally, the DL2 damage scenario also collapsed at $\lambda_{damaged}$ equal to 0.896 corresponding to a RRI value of -0.023. The negative RRI value indicates that the damaged structure cannot support its intended design loads. The extent of damage to the structure at collapse represented by the formation of plastic hinges is shown in Figure

23a and 23b for the undamaged and single column removal cases, respectively. Beam hinges that have reached the CP acceptance level are shown in yellow. Red hinges indicate where a column has exceeded its axial capacity and thus has begun to rapidly displace downward.

These results show that the distribution of damage to the frame without any column removals reduces the RRI when compared to that of the completely undamaged frame by approximately 28%. The notional single column removal case and the scenario where a column is removed with adjacent damage both result in the same RRI. This can be attributed to the failure mechanisms developing faster in the bays above the removal than the axial load redistribution to the adjacent columns. A few design changes may influence the level of load at which the primary failure mechanism changes from the development of CP hinges in the beam to overload of the adjacent columns. Most notably, an enhancement of the moment connection strength can delay the formation of CP hinges, and thus redistributing additional axial load to the adjacent columns. Also, a reduction in the capacity of the adjacent column can allow for its overload to occur sooner. For this case study, it was determined that for the mechanism to shift, either the moment connection strength would need to be amplified by a factor of 3 or the adjacent column would exhibit a residual axial capacity of less than 3,559 kN (800 kips). Also, buildings not specifically detailed for seismic regions may also exhibit lesser resilience to progressive collapse.

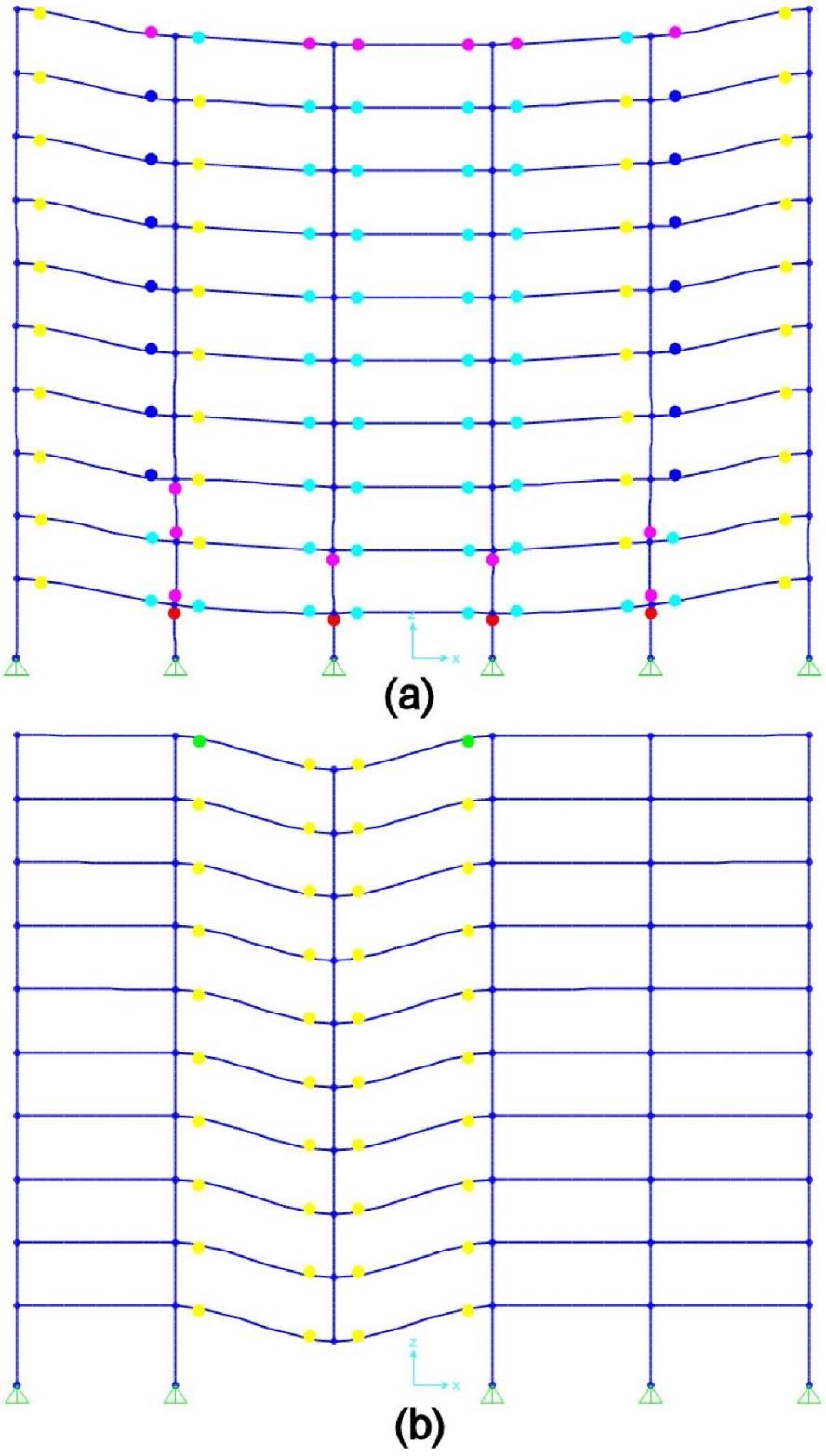

Figure 23 - Extent of plastic hinge formation at collapse for the undamaged case (a) and the one column removal (b)

SUMMARY AND CONCLUSIONS

This paper presents a framework for mapping blast-induced damage both as contours on the surface of a reinforced concrete building frame and as standoff boundaries on the site surrounding the structure to assess the damage to the exterior load carrying system. These threat-dependent damage maps can be used as part of a coupled progressive collapse vulnerability assessment of structures. The contours are a visual representation of the blast-induced damage levels and are a function of reflected pressure and impulse loading and the material and geometric properties of the concrete columns. This model can be used to evaluate the final damage state of the critical column locations for flexure, direct shear, and breach failure modes. By visually assessing the damage contours and their boundaries relative to the location of critical columns within the building frame, the extent of blast-induced damage to all columns can be evaluated. The number of columns to be removed when analyzing the progressive collapse potential of a building frame depends on how many column lines fall within the breach or blowout failure contours. Utilizing the developed methodology, one can demonstrate the potential for multiple column removals for a range of explosive threats.

A case study was performed to illustrate the applicability of the proposed framework. A 10-story prototype reinforced concrete moment frame building was subjected to blast-induced pressure loading for a range of explosive threats, and the response of all perimeter columns was evaluated. A set of hazards was examined, representing a range of TNT charge sizes and standoff distances. A second set of trials varied the standoff location of three different charge sizes on the ground surface in front of the building frame.

When the prototype building frame was subjected to the spatial distribution of blast-induced damage for set of hazards, it was shown that the building exhibits a reduction in overall robustness when compared to the building that is completely undamaged. The same robustness was exhibited for both cases of the notional single column removal approach (with and without adjacent damage) due to the development of CP hinges in the beams above the removal.

The results of this study indicate that when coupled with the effects of blast loading, the current alternate path method for progressive collapse analysis (which utilizes the one column removal approach) may be non-conservative for a relatively wide range of explosive threat sizes and locations. The damage contours show that multiple columns can suffer breach when subjected to large charge sizes at small standoff distances. Cases where a single column is removed are shown to also result in significant damage to adjacent columns. Even in cases where no columns are removed, significant damage can occur to the building frame, potentially compromising its structural integrity and collapse resistance. This study suggests that a threat-dependent approach may enable the design of high-risk facilities to the levels of robustness needed to resist realistic consequences of blast-induced damage.

REFERENCES

ACI (2011). ACI 318-11: Building Code Requirements for Structural Concrete and Commentary. American Concrete Institute, Farmington Hills, MI.

ASCE (2007). *ASCE/SEI 41-06: Seismic Rehabilitation of Existing Buildings.* American Society of Civil Engineers, Reston, Va.

ASCE (2010). ASCE 7-10: Minimum design loads for buildings and other structures. American Society of Civil Engineers, Reston, Va.

Asprone, D., Jalayer, F., Prota, A., and Manfredi, G. (2010). "Proposal of a probabilistic model for multi-hazard risk assessment of structures in seismic zones subjected to blast for the limit state of collapse." *Struct. Saf.*, 32, 25–34.

Astarlioglu, S., Krauthammer, T., Morency, D., Tran, T.P. (2013). "Behavior of reinforced concrete columns under combined effects of axial and blast-induced transverse loads." *Engr. Struct.*, 55, 26-34.

Bao, X., and Li, B. (2010). "Residual strength of blast damaged reinforced concrete columns." *Int. J. Impact Eng.*, 37, 295-308.

Biggs, J.M. (1964). Introduction to Structural Dynamics. McGraw-Hill.

Byfield, M. and Paramasivam, S. (2012). "Murrah Building Collapse: Reassessment of the Transfer Girder." *J. Perform. Constr. Facil.*, 26(4), 371–376.

Corley, W., Mlkar, P., Sozen, M., and Thornton, C. (1998). ”The Oklahoma City Bombing: Summary and Recommendations for Multihazard Mitigation.” *J. Perform. Constr. Facil.*, 12(3), 100–112.

CSI (2014). SAP2000 v17.1.1. Computers & Structures, Inc. Walnut Creek, CA.

DoD. (2014). UFC 3-340-02: Structures to resist the effects of accidental explosions. US Department of Defense, Washington, DC.

DoD (2013a). UFC 4-010-01: DoD minimum antiterrorism standards for buildings. US Department of Defense, Washington, DC.

DoD (2013b). UFC 4-023-03: Design of buildings to resist progressive collapse. US Department of Defense, Washington, DC.

Dragos, J., and Wu, C. (2014). “Interaction between direct shear and flexural responses for blast loaded one-way reinforced concrete slabs using a finite element model.” *Engr. Struct*., 72, 193-202.

Fallon, C., Quiel, S., and Naito, C. (2016). “A Uniform Pushdown Approach for Quantifying Building Frame Robustness and the Consequence of Disproportionate Collapse.” *J. Perform. Constr. Facil.,* Accepted for Publication.

GSA (2013). Alternate path analysis & design guidelines for progressive collapse resistance. General Services Administration. Washington, DC.

ICC (2012). *2012 International Building Code*. International Code Council, Country Club Hills, Ill.

Kazemi-Moghaddam, A., and Sasani, M. (2015). “Progressive collapse evaluation of Murrah Federal Building following sudden loss of column G20.” *Engr. Struct*., 89, 162-171.

Kelliher, D., and Sutton-Swaby, K. (2012). “Stochastic representation of blast load damage in a reinforced concrete building.” *Struct. Saf.*, 34(1), 407–417.

Krauthammer, T., Bazeos, N., and Holmquist, T. (1986). ”Modified SDOF Analysis of RC Box Type Structures.” *J. Struct. Eng.*, 112(4), 726–744.

Lew, H.S., Bao, Y., Sadek, F., Main, J.A., Pujol, S., and Sozen, M.A. (2011). *TN-1720: An Experimental and Computational Study of Reinforced Concrete Assemblies under a Column Removal Scenario*. National Institute of Standards and Technology (NIST), Gaithersburg, MD.

Low, H.Y., and Hao, H. (2002). “Reliability analysis of direct shear and flexural failure modes of RC slabs under explosive loading.” *Engr. Struct*., 24, 189-198.

Luccioni, B.M., Ambrosini, R.D., and Danesi, R.F. (2004). “Analysis of building collapse under blast loads.” *Engr. Struct*., 26, 63-71.

McConnell, J.R., and Brown, H. (2011). “Evaluation of progressive collapse alternate load path analyses in designing for blast resistance of steel columns.” *Engr. Struct*., 33, 2899-2909.

Mlakar, P., Corley, W., Sozen, M., and Thornton, C. (1998). ”The Oklahoma City Bombing: Analysis of Blast Damage to the Murrah Building.” *J. Perform. Constr. Facil.*, 12(3), 113–119.

Myers, G. and Crawford, J. (2014). “Effectively Addressing the Risks to the Infrastructure Presented by Extreme Hazards: The Need for a Shift in the Design Paradigm.” *Proc. ICSI 2014*, 903-909.

Nair, R. (2006). ”Preventing Disproportionate Collapse.” *J. Perform. Constr. Facil.* 20, 309–314.

Netherton, M.D., and Stewart, M.G. (2009). “The effects of explosive blast load variability on safety hazard and damage risks for monolithic window glazing.” *Int. J. Impact Eng*., 36, 1346-1354.

Osteraas, J. (2006). ”Murrah Building Bombing Revisited: A Qualitative Assessment of Blast Damage and Collapse Patterns.” *J. Perform. Constr. Facil.*, 20, 330–335.

Quiel, S., Marjanishvili, S., and Katz, B. (2015). "Performance-Based Framework for Quantifying Structural Resilience to Blast-Induced Damage." *J. Struct. Eng.*, accepted for publication.

Sasani, M. (2008). “Response of a reinforced concrete infilled-frame structure to removal of two adjacent columns.” *Engr. Struct*., 30, 2478-2491.

Sasani, M., Kazemi, A., Sagiroglu, S., and Forest, S. (2011). ”Progressive Collapse Resistance of an Actual 11-Story Structure Subjected to Severe Initial Damage.” *J. Struct. Eng.,* 137, 893–902.

Shi, Y., Li, Z., and Hao, H. (2010). “A new method for progressive collapse analysis of RC frames under blast loading.” *Engr. Struct*., 32, 1691-1703.

Starossek, U. and Haberland, M. (2010). ”Disproportionate Collapse: Terminology and Procedures.” *J. Perform. Constr. Facil.*, 24(6), 519–528.

Stewart, M.G., Netherton, M.D., Rosowsky, D.V. (2006). “Terrorism risks and blast damage to built infrastructure.” *Nat. Haz. Rev.*, 7(3), 114-122.

Timoshenko, S.P. and Gere, J.M. (1961). *Theory of Elastic Stability (2nd Ed.).* McGraw-Hill.

US Army Corps of Engineers. (2008a). PDC TR-06-01: Methodology Manual for the Single-Degree-of-Freedom Blast Effects Design Spreadsheets (SBEDS) (Rev 1), US Army Corps of Engineers, Vicksburg, MS.

USACE (2008b). PDC TR-06-08: Single Degree of Freedom Structural Response Limits for Antiterrorism Design (Rev 1), US Army Corps of Engineers, Vicksburg, MS.

Wei, W., Duo, Z., Fang-yun, L., Fu-jing, T., and Song-chuan, W. (2013). “Pressure-impulse diagram with multiple failure modes of one-way reinforced concrete slab under blast loading using SDOF method.” *J. Cent. South Univ*., 20, 510-519.

Williamson, E.B., Bayrak, O., Williams, G.D., Davis, C.E., Marchard, K.A., McKay, A.E., Kulicki, J., and Wassef, W. (2010). *NCHRP Report 645: Blast-Resistant Highway Bridges: Design and Detailing Guidelines*. National Cooperative Highway Research Program (NCHRP), Washington, DC.

Xu, J., Wu, C., and Li, Z. (2014). "Analysis of direct shear failure mode for RC slabs under external explosive loading." *Int. J. Impact Eng*., 69, 136-148.

AUTHOR BIOGRAPHY

Matthew Jonathan Gombeda was born in Hazleton, Pennsylvania on December 13, 1991 to parents Mark and Paula Gombeda. He is a 2010 graduate of Hazleton Area High School. Matt received a Bachelor of Science degree in civil engineering and a minor in engineering mechanics from the Pennsylvania State University in 2014. After graduating, he will remain at Lehigh to pursue a PhD in structural engineering.